January 2001 ANL/TD/TM01-16

Assessment of the General Atomics Accelerator Transmutation of Waste Concept Based on the Gas-Turbine-Modular Helium Cooled Reactor Technology

by

Yousry Gohar, Temitope A. Taiwo*, James E. Cahalan*, and Phillip J. Finck

Technology Development Division
*Reactor Analysis and Engineering Division

Argonne National Laboratory
9700 South Cass Avenue
Argonne, IL 60439

Work supported by the
Office of Nuclear Energy, Science & Technology
U.S. Department of Energy
under Contract W-31-109-Eng-38

Available electronically at http://www.doe.gov/bridge

Available for a processing fee to U.S. Department of Energy and its contractors, in paper, from:

U.S. Department of Energy
Office of Scientific and Technical Information
P.O. Box 62
Oak Ridge, TN 37831-0062
phone: (865) 576-8401
fax: (865) 576-5728
email: reports@adonis.osti.gov

Table of Contents

List of Figures

LIST OF TABLES

Assessment of the General Atomics Accelerator Transmutation of Waste Concept Based on the Gas-Turbine-Modular Helium Cooled Reactor Technology

Yousry Gohar, Temitope A. Taiwo, James E. Cahalan, and Phillip J. Finck

Abstract

An assessment has been performed for an Accelerator Transmutation of Waste (ATW) concept based on the use of the high temperature gas reactor technology. The concept has been proposed by General Atomics for the ATW system. The assessment was jointly conducted at Argonne National Laboratory (ANL) and Los Alamos national laboratory to assess and to define the potential candidates for the ATW system. This report represents the assessment work performed at ANL.

The concept uses recycled light water reactor (LWR)-discharge-transuranic extracted from irradiated oxide fuel in a critical and sub-critical accelerator driven gas-cooled transmuter. In this concept, the transmuter operates at 600 MW_t first in the critical mode for three cycles and then operates in a subcritical accelerator-driven mode for a single cycle. The transmuter contains both thermal and fast spectrum transmutation zones. The thermal zone is fueled with the TRU oxide material in the form of coated particles, which are mixed with graphite powder, packed into cylindrical compacts, and loaded in hexagonal graphite blocks with cylindrical channels; the fast zone is fueled with TRU-oxide material in the form of coated particles without the graphite powder and the graphite blocks that has been burned in the thermal region for three critical cycles and one additional accelerator-driven cycle. The fuel loaded into the fast zone is irradiated for four additional cycles. This fuel management scheme is intended to achieve a high Pu isotopes consumption in the thermal spectrum zone, and to consume the minor actinides in the fast-spectrum zone.

Monte Carlo and deterministic codes have been used to assess the system performance and to determine the feasibility of achieving high TRU consumption levels. The studies revealed the potential for high consumption of Pu-239 (97%), total Pu (71%) and total TRU (64%) in the system. The analyses confirmed the need for burnable absorber for both suppressing the initial excess reactivity and ensuring a negative temperature coefficient under all operating conditions. Additionally, current results suggest that it may be preferable to use a double strata thermal critical system and fast subcritical system to achieve nearly complete destruction of the TRU oxide fuel.

The report gives a general description of the system proposed by General Atomics. The major design parameters (degrees of freedom), which can be altered to optimize the system design, and the constraints, which guide the design and the optimization studies are described. The deterministic and the Monte Carlo neutronics codes and models used for the neutronics analysis and assessment are presented.

The results of fuel block and whole-core parametric studies performed to understand the physics are given including the effect of various fuel management schemes on the system performance. A point design is described including the system performance results for a single-batch and three-batch loading schemes. The major design issues, which need to be addressed during further studies, are discussed.

I. Introduction

General Atomics (GA) has proposed an Accelerator Transmutation of Waste (ATW) concept based on a variant of the gas-turbine-modular helium cooled reactor (GT-MHR) [1]. This report describes the assessment work of that concept, performed by the Argonne National Laboratory (ANL) team. The report also lists the major issues, which need to be addressed during further phases of the ATW roadmap implementation.

A general description of the system proposed by GA is presented in Section II. The major design parameters (degrees of freedom), which can be altered to optimize the system design, and the constraints, which guide the design and optimization studies are described in Section III. The computer codes and the geometrical models used for the neutronics evaluation, and the main parameters of the proposed system are presented in Section IV. Overviews of the parametric studies, which have been performed to understand the neutronics performance of the basic design, are given in Section V. The effect of various fuel management schemes on the system performance is given in Section VI. A point design is described in Section VII including the system performance results. Section VIII discusses the major issues, which need to be addressed during further studies.

II. System Description

A general layout of the system proposed by GA is shown in Figures 1 and 2. The transmuter consists of a steel vessel housing, containing an annular transmutation region operating with a thermal neutron spectrum. This annular region contains the "fresh" transuranic materials (TRU) separated from light water reactor (LWR) spent fuel. The TRU are contained in spherical TRISO-coated particles. These spherical particles consist of a 200μm diameter $TRUO_{1.7}$ core, called kernel, surrounded by layers of graphite buffer (thickness 100μm) to absorb gaseous fission products, pyrolitic graphite (thickness 35μm), silicon carbide (thickness 35μm) to serve as a stable barrier and pressure vessel, and an outside layer of pyrolitic graphite (thickness 40μm). These particles are mixed with graphite powder and packed into cylindrical compacts. The compacts are loaded into cylindrical channels within hexagonal graphite blocks, as shown in Figure 3. The blocks also have channels for helium coolant flow and channels for introducing erbium burnable poison into the system. The blocks are 36 cm flat-to-flat, and contain 202 TRU channels, 108 coolant channels and 14 burnable poison (BP) channels, all arranged on a 1.88-cm triangular pitch. TRU blocks are loaded into the fifth, sixth, and seventh radial rings of a hexagonal configuration. Three rings of graphite reflector are arranged both inside and outside this thermal region. The innermost layer is filled with fast TRU assemblies, composed of the TRU particles that has undergone four years of burning in the thermal region. The vertical configuration comprises ten active blocks stacked vertically. The fast blocks have not yet been designed, and for the purpose of this study it is assumed that they are similar to the Gas Cooled Fast Reactor (GCFR)

design developed in the 70's and early 80's. At the center of the configuration is the location for a spallation target used during the period of subcritical operation.

The transmuter operates in the critical mode for approximately three years, which corresponds to 75% of the cycle length. In this mode, the critical thermal region drives the fission process and limited transmutation events are expected in the fast region. After these three years, the thermal region becomes subcritical and is driven by the spallation target neutrons during the fourth year of the cycle. The local multiplication of spallation neutrons in the fast region might produce a significant fast flux thus helping the transmutation of the minor actinides. The plant would comprise four 600 MWth transmuters, sharing one 15-MW beam accelerator.

The transmuter is cooled by helium with an outlet temperature of 850 °C. The heated helium is used in a direct-cycle gas-turbine-generator system. The high operating temperatures and the characteristics of the direct Brayton power conversion system allow electric generation with a high net thermal efficiency of about 47%.

Preliminary analyses by GA [1] indicate that this design will achieve high levels of transmutation without requiring reprocessing, due to the endurance of the coated particles containing the TRU under neutron irradiation conditions.

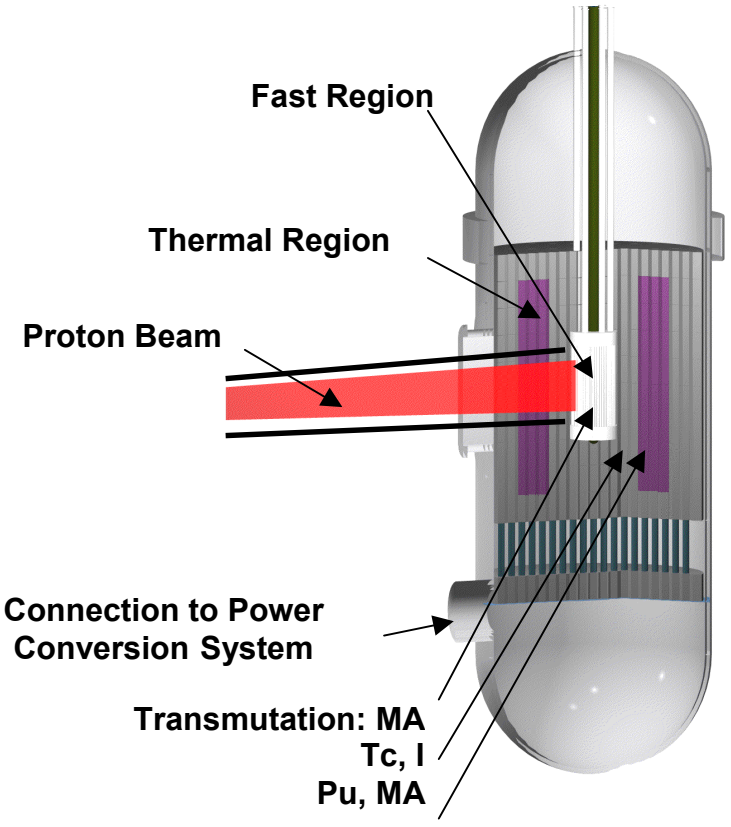

Figure 1. Thermal fast transmuter

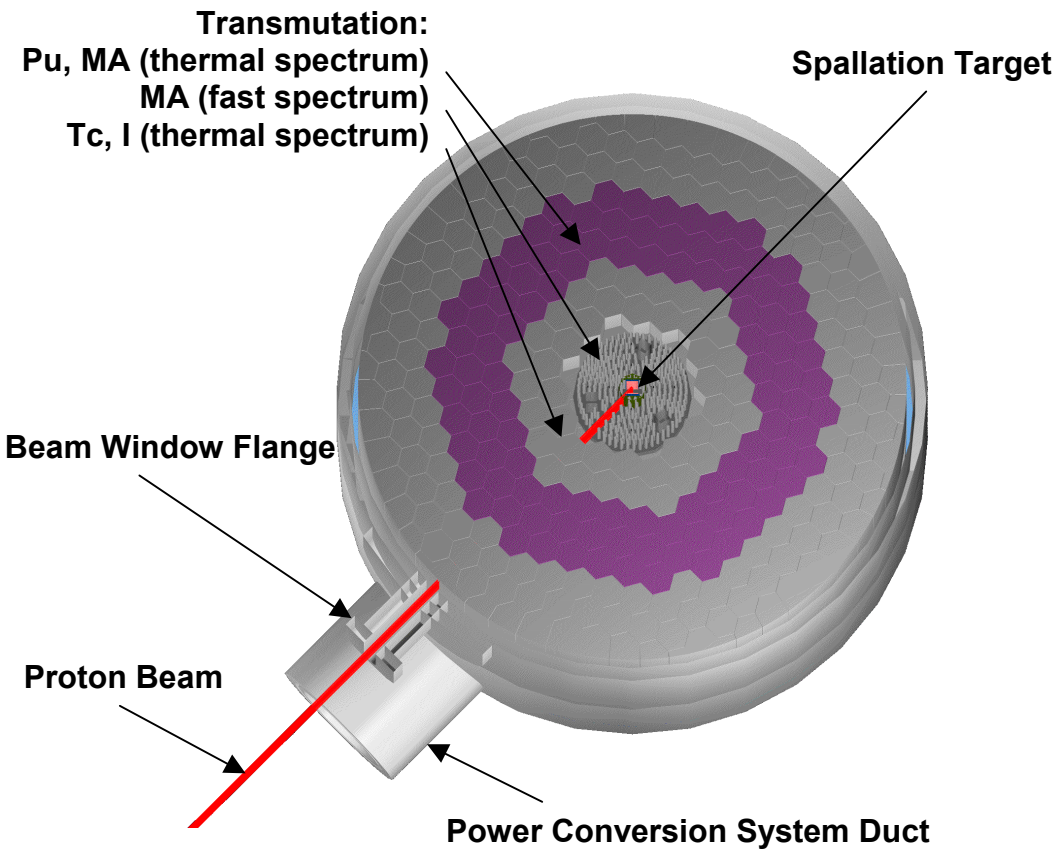

Figure 2. Thermal-fast transmuter cross section

III. Objectives, Constraints, and Degrees of Freedom

The main objectives of the system design activities are the following:

- Achieve very high burnup of the initial loading of plutonium and minor actinides;
- Maintain fuel particle integrity throughout the fuel cycle and into disposal, thus avoiding the need for intermediate reprocessing;
- Maintain high operating temperatures needed to achieve a high net thermal efficiency.

Several constraints are taken into consideration for the system design process including the following:

- TRU material performance: this issue is addressed in section X. It should be noted that the very high burnup levels considered for this system are beyond the limits of the available experimental database.

- Safety: safety must be guaranteed at all times, in particular during critical operation. The TRU contains relatively little resonant absorbers, as compared to traditional LWR fuel. Thus, the fast acting Doppler coefficient might become quite small; the addition of erbium burnable poison will help create a moderator temperature effect, but this might also be offset by the erbium consumption during operation.

- TRU operating temperature: TRU materials must remain within their nominal temperature ranges during both subcritical and critical stages. While the MHR design has been well studied, several new features of the system might make it more difficult to cool. The high burnup of the TRU material might create large power peaks in the thermal region. Also, the subcritical operation might create large power peaks in the fast region and the design of the fast region needs to consider carefully the temperature range of the TRU material during the different operating stages including transient conditions.

- Reactivity Control: the high burnup objective implies significant changes in the TRU material inventory during operation. If a simple TRU management system is used, this can result in significant reactivity changes during the transmutation cycle. The use of control rods, burnable poisons, or accelerator power grading are required to control the change of the system reactivity. As much as possible, it is desirable to reduce the reactivity changes during operation.

- Cycle length: it is usually desirable to achieve long cycle length to reduce the plant down time. Furthermore, it is beneficial to increase the critical cycle length and decrease the subcritical cycle length to reduce the accelerator power requirements.

For the purpose of this study, it was decided to limit the degrees of freedom available to the designers, the current study parameters remain relatively close to the design database developed by GA over the past decades. In the future, it might become of interest to allow for significant flexibility in the design parameters. The following parameters are fixed:

- TRU block geometry as defined in Figure 3.
- Configuration and overall dimensions as defined in Figures 1 and 2.
- Power level (600 MWth) and operating temperatures, as described by GA [1].

Nevertheless, the effect of several other design parameters on the system performance is analyzed. The initial heavy metal loading, the initial erbium burnable poison loading, the loading pattern (number of fuel blocks), and the fuel management scheme are expected to have an effect on initial reactivity, cycle length, temperature coefficient, and achievable burnup. The effects of these degrees of freedom on fuel block and system performances are described in Sections VI through VII.

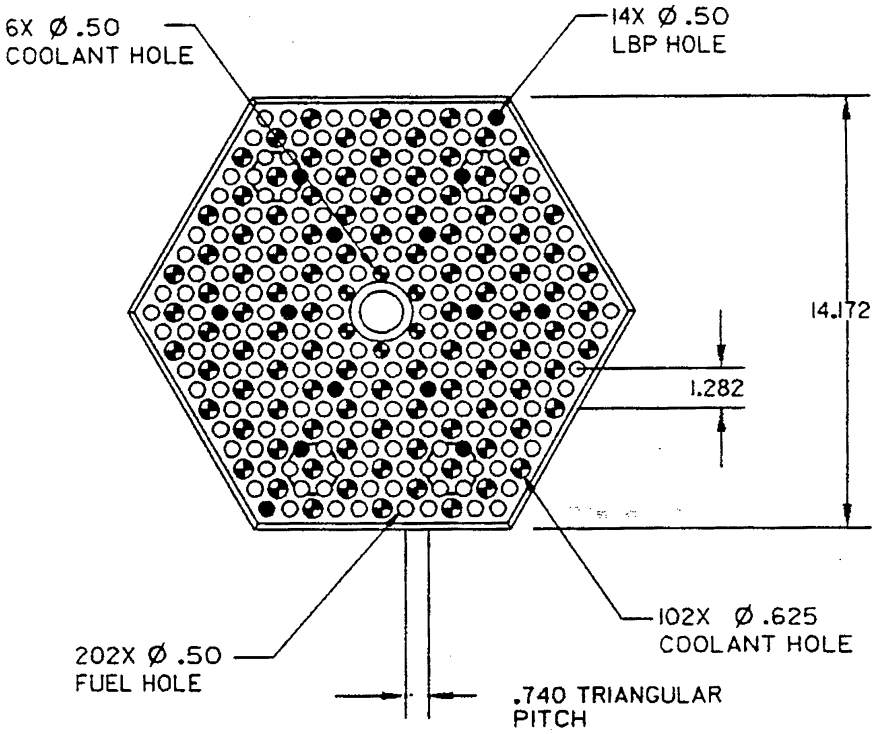

Figure 3. Cross-sectional view of the thermal block, dimensions in inches

IV. Computer Codes Used for Neutronics Analyses

Two independent computational paths have been implemented for the GT/AD-MHR studies:

- A deterministic path based on the DRAGON [4], DIF3D [5], and REBUS [6] computer codes has been utilized. It promises fast computer running times and allows for multiple perturbation calculations, but it relies on a series of energetic and spatial homogenization steps which might decrease the accuracy of the results. Thus, it needs to be carefully validated.

- An independent stochastic path based on MONK computer code [2] has been utilized. It is also used to check the predictions of the deterministic path and to provide a reference database. A report [3] is being prepared to document the results and to provide a reference database for future work

V. Calculational Models Used for Neutronics Analyses

The GT/AD-MHR design includes several levels of heterogeneity effects that require proper treatment in order to obtain accurate performance predictions for the system. The fuel elements are hexagonal prismatic blocks of graphite containing parallel vertical holes, arranged in a triangular pitch. These holes contain TRU or BP

compacts and some vacant holes for coolant flow paths. Other holes are utilized for control rods and fuel loading devices, but have not been modeled in this study. The TRU and BP compacts consist of multi-layer ceramic-coated particles dispersed in a graphite matrix. Significant neutronics heterogeneities are created by these small particles. Fuel block heterogeneity arising from the heterogeneous arrangement of TRU, BP and coolant channels in the element, also exists in this design. Another geometrical heterogeneity is also present because of the annular configuration that employs inner and outer reflector zones, and the fast and thermal core zones. Configuration data are presented in Table I.

The heterogeneities have been evaluated using Monte Carlo and deterministic models. The Monte Carlo model is based on the MONK computer code, which employs JEF2.2 nuclear data library. A deterministic scheme based on the DRAGON lattice computer code [4], the ENDF/B-VI nuclear data library, and the DIF3D/REBUS3 [5 and 6] suite of fission reactor analysis codes has also been developed. In order to verify the accuracy of the deterministic code predictions, the results of homogeneous-cell, heterogeneous-cell, and whole configurations performed with these codes have been compared to those obtained with the MONK computer code or other deterministic codes. Similar effort is required to validate the burnup results.

V.1. Thermal Block Model

Burnup-dependent, block-average microscopic cross-sections are obtained using the DRAGON lattice computer code and an ENDF/B-VI based 69-group library. The DRAGON computer code is selected because it models accurately the dispersion fuel in a graphite matrix and permits full-block calculations using the collision probability method. Resonance self-shielding and depletion calculations in the particles are possible because DRAGON allows explicit representations of the multi-layer TRU and BP particles, the matrix graphite, and the block graphite of the GT-MHR design.

The need to provide an explicit model for the fuel block was assessed using the MONK computer code. MONK has the capability to explicitly model the geometry under consideration and to perform criticality and burnup analyses in an integrated manner. The particles are modeled as a hexagonally close-packed lattice of spheres. The lattice forms a regular octahedron and it is cut by a cylinder to represent the compact. MONK criticality calculation can be performed with quasi-continuous energy or multigroup data sets. The quasi-continuous energy data set is processed in a fine energy mesh (13193 or 8220 groups). The multigroup libraries are processed in a much coarser set (172 or 69 groups). The burnup analyses use the coarser data sets. The nuclear data libraries are based on JEF version 2.2. Three different models for representing the TRU or the BP compacts in the TRU block were evaluated. These are:

Table I. GT/MHR configuration parameters

Parameter	Value
TRU Kernel Properties	
Form, Density	$TRUO_{1.7}$, 10.2 g/cc
Diameter	200 μm
TRU Particle Coating Properties	
Buffer, Density	100 μm, 1.00 g/cc
Inner Dense PyC, Density	35 μm, 1.87 g/cc
SiC, Density	35 μm, 3.20 g/cc
Outer Dense PyC, Density	40 μm, 1.83 g/cc
Particle Diameter	620 μm
Erbium Kernel Properties	
Form, Density	Er_2O_3, 8.64 g/cc
Diameter	400 μm
Erbium Particle Coating Properties	
Buffer, Density	100 μm, 1.00 g/cc
Inner Dense PyC, Density	35 μm, 1.87 g/cc
SiC, Density	35 μm, 3.20 g/cc
Outer Dense PyC, Density	40 μm, 1.83 g/cc
Particle Diameter	820 μm
TRU Heavy Metal Composition	
Np-237	4.10%
Pu-238	1.20%
Pu-239	51.55%
Pu-240	23.88%
Pu-241	7.99%
Pu-242	5.00%
Am-241	5.00%
Am-242M	0.10%
Am-243	1.00%
Cm-242	0.00%
Cm-243	0.00%
Cm-244	0.20%
Cm-245	0.00%
Configuration Temperatures	
Average Thermal Assembly TRU Temperature	770 ^{o}C
Temperature Operating Range	580 ^{o}C to1250^{o}C
Average Graphite Temperature	700 ^{o}C
Average Fast Assembly Fuel Temperature	770 ^{o}C
Thermal Assembly TRU Element Data	
TRU Element Pitch (includes gaps)	36.1 cm
TRU Element Height	79.3 cm
Graphite Block Density	1.74 g/cc
Number of TRU and BP Holes	216
Hole Diameter	1.27 cm
Compact Diameter	1.2446 cm
Coolant Holes	
Number of Inner/Outer Holes	6/102
Diameter Inner/Outer Holes	1.27/1.5875 cm

- Explicit modeling of the block including the multi-layer fuel and the BP particles inside the compacts as shown in Figures 4 through 6.
- Block model using a homogeneous mix of the particle layers inside the compact (homogenized particles).
- Block model employing a homogeneous mix of particle layers and matrix graphite (homogenized compact).

The difference in the k_∞ of the thermal block, between the first and either of the two models provide an estimate of the heterogeneity effect due to the particles in the compact. Table II summarizes the MONK results using the quasi-continuous energy nuclear data library (13193 groups) for a case employing a heavy-metal loading of 771 grams per block. The composition and density of each material are given in Table 1. In this MONK analysis, it was assumed that the fuel block is loaded with fuel compacts and helium coolant channels, without erbium burnable poison compacts and without the block-handling hole. The MONK results show a strong heterogeneity effect. The DRAGON model similarly predicted this effect to be 14% for $\Delta k_\infty/k_\infty$.

Table II. TRU compact heterogeneity effect

Computer Code	MONK	
TRU Model	k_∞	$\Delta k_\infty/k_\infty$, %
Explicit Modeling	1.2764	--
Homogenized Particles	1.1101	-13.02
Homogenized Compact	1.0928	-14.38

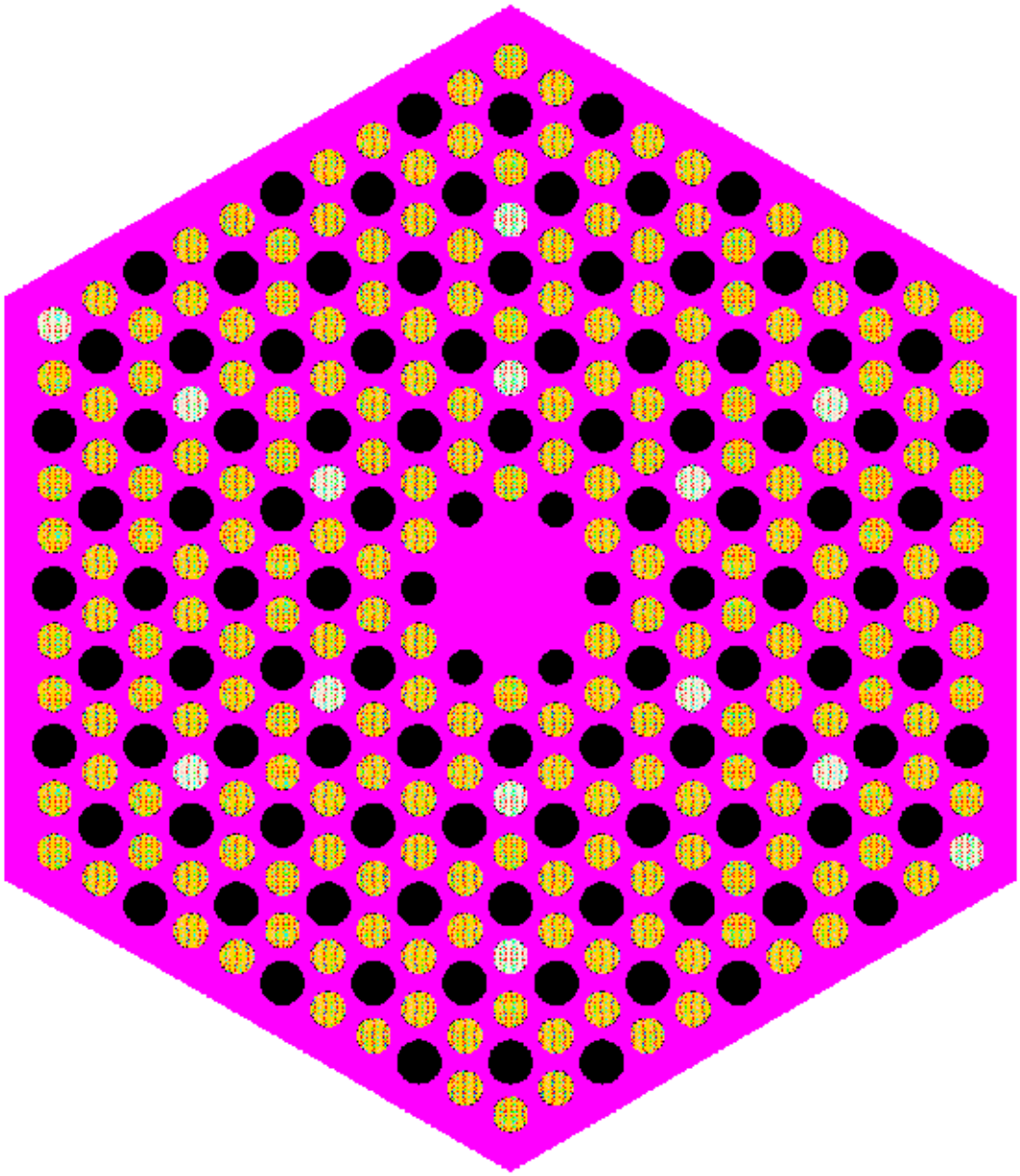

Figure 4. Thermal block model

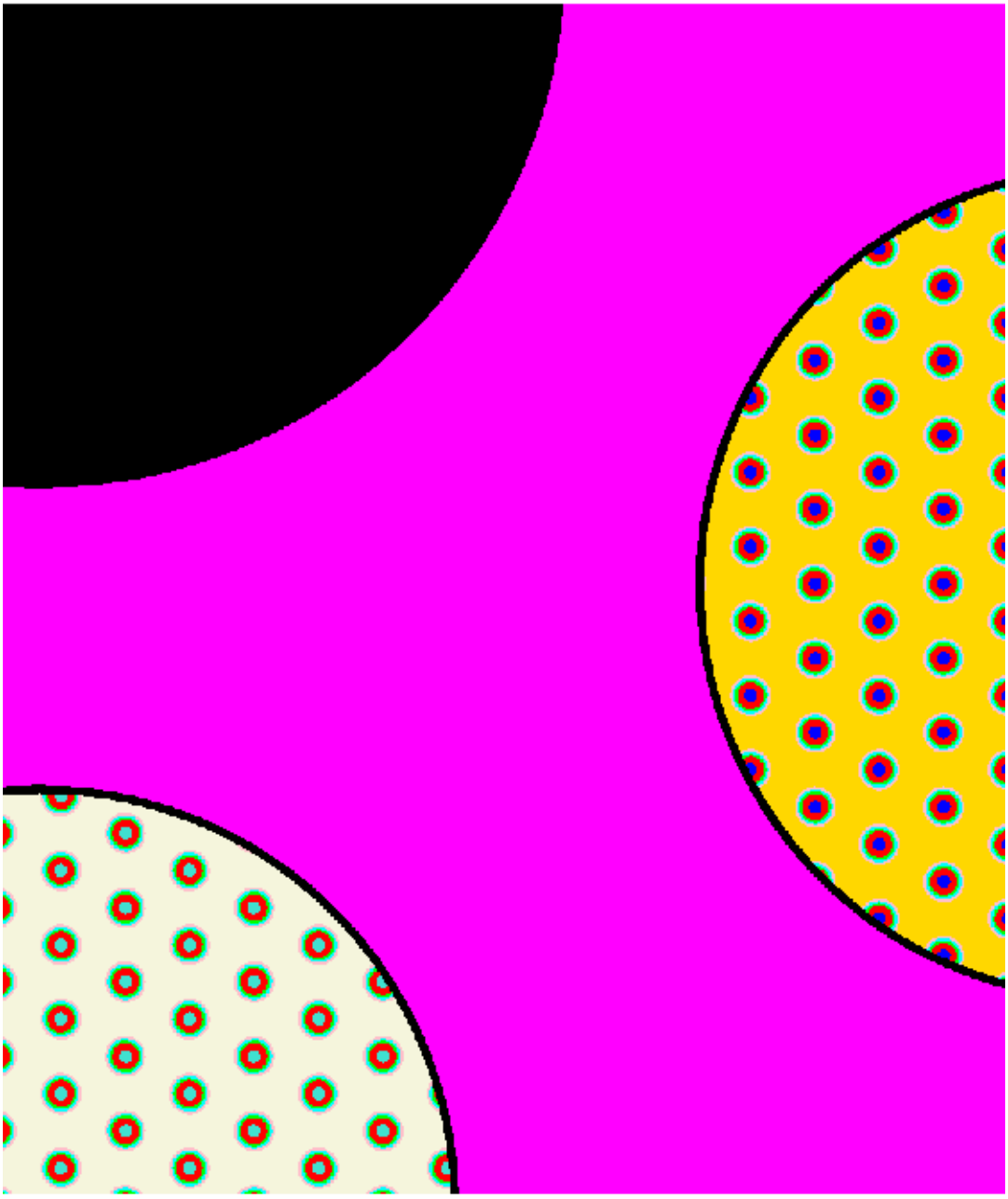

Figure 5. Enlarged block section featuring a section of the coolant channel (Top left), TRU compact (Right), and burnable poison compact (Bottom left)

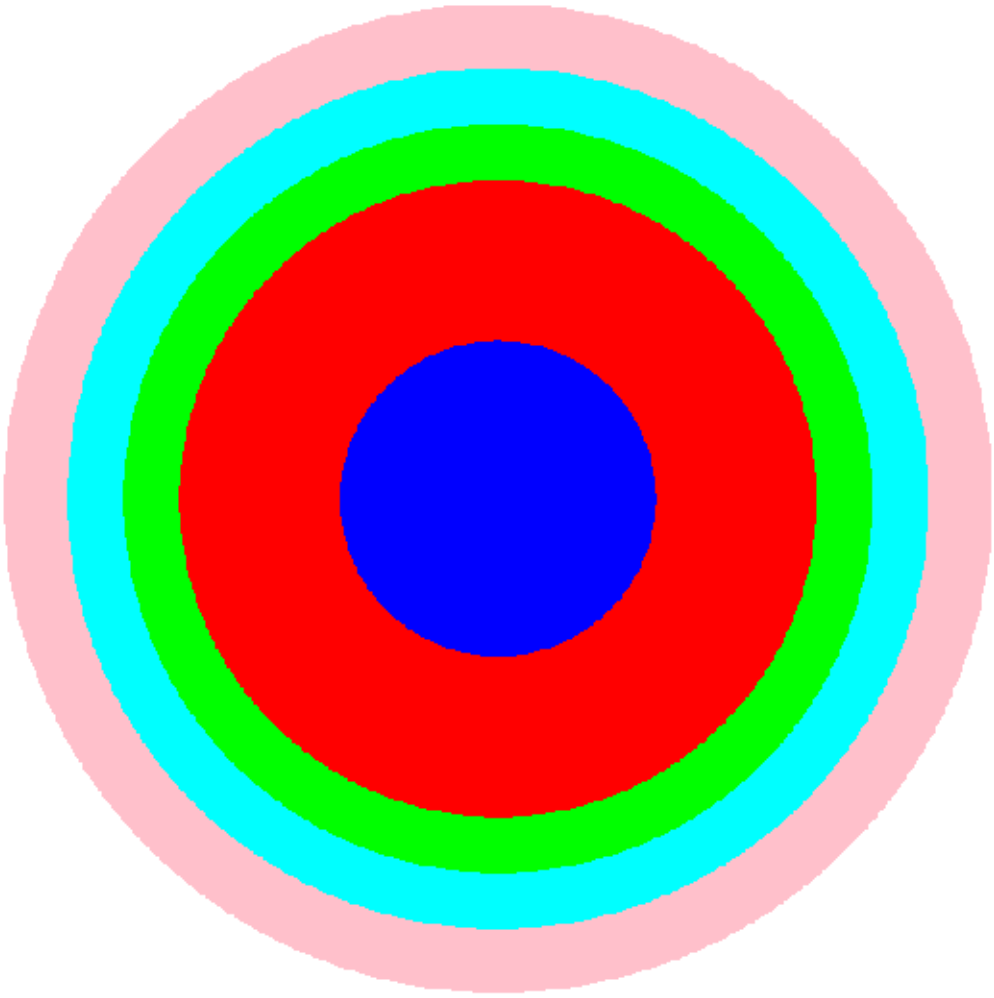

Figure 6. Fuel particle model

The detailed block model shown in Figure 3 is used to study the BP heterogeneity effect. The volume packing fractions for the fuel and the BP particles are 0.1238 and 0.1, respectively. The MONK computer code with the quasi-continuous energy nuclear library (13193 groups) based on JEF2.2 was used for the analysis. Similar to the TRU analysis, three cases were analyzed for the BP modeling. The particle homogenization under predicts k_∞ by about -1.8% relative to the explicit modeling as shown in Table III. The homogenized compact increases the discrepancy to -2.2%. These results are consistent with the fuel heterogeneity results obtained before. In this case, the self-shielding change caused by the erbium absorption resonance explains the change in k_∞ of the block, which explained in the next paragraph. The burnable poison heterogeneity effect is smaller than the corresponding value for the TRU because the block has only 14 BP compacts relative to 202 TRU compacts.

The homogeneous models give inaccurate k_∞ values because these models significantly under predict the self-shielding of the strong absorption resonances in the plutonium isotopes, particularly Pu-240, and Er-167 in the BP. This is caused by the

fact that the fuel and the BP particle dimensions are relatively large compared to the mean free path of neutrons in the low-energy-lying resonances of these isotopes. Because of this effect, the inner zone of the particle is shielded from neutrons by the outer zone and simple homogenization of cross sections does not account correctly for the self-shielding effect. For both the fuel and BP compact cases, the heterogeneity effect was found to be dependent on the particle composition and the packing fraction. The difference in k_∞ between the homogeneous and explicit models decreases as the packing fraction increases for fixed particle size or as the fuel radii decreases for fixed packing fraction.

Table III. MONK burnable poison heterogeneity effect

Burnable Poison Model	k_∞	$\Delta k_\infty/k_\infty$, %
Explicit Modeling	1.1864	
Homogenized Particles	1.1649	-1.81
Homogenized Compact	1.1604	-2.19

Fuel block power distributions predicted by MONK and DRAGON have also been compared. The comparison for a fuel block containing 14 BP compacts at the cold state (293 K) indicated that DRAGON accurately predicts the power distribution in the block. The difference in the maximum power density of the TRU compact predicted by the two computer codes is about 1.1%. The maximum power in this case occurs in a TRU compact located close to the block boundary because of the extra (non-cell) graphite present in this zone, which causes a softer neutron spectrum. The maximum difference in the TRU compact power is about 2.9% and occurs for a TRU compact operating close to the average block power and also neighboring a coolant channel at the inner block ring.

In summary, the DRAGON and the MONK computer codes give consistent results on a series of calculations from simple compact cell to full block analyses. These results provide confidence in the validity of the deterministic calculations. The strong double heterogeneity effects observed for the fuel and erbium particles imply that a detailed modeling of these particles will be required for the analyses.

The depletion model for the GT-MHR cell has been verified by comparing results from DRAGON to those obtained with the WIMS8 deterministic code. The cell calculations were done primarily to check the performance of DRAGON compared to another deterministic code, which also employs a different cross-section library (JEF-2.2 versus ENDF/B-VI used in DRAGON). The WIMS8 computer code has been used and validated for evaluating high-temperature gas-cooled reactor systems employing particulate fuel in graphite matrix, and hence is adequate for the

comparison. The two codes predicted very similar k-infinities for an at-power conditions in which the fuel particles and matrix graphite were explicitly represented and another case in which they were smeared together into a single composition. The WIMS8 depletion chain was judged to be superior because it modeled more transmutation events; the modeling of transmutation events by DRAGON is limited only by the information available in the cross section library. The two computer codes however gave very similar trend of k-infinity with burnup for a constant-flux depletion case. For this case, the codes predicted practically the same time evolutions of the number densities of the primary nuclides. The slight differences in the time evolutions of the number densities of Pu-238 and Pu-242 were attributed to the differences in the depletion chains.

V.2. Transmuter Models

Two three-dimensional transmuter models were developed for performing the neutronics calculations of this study. The first is a deterministic model for DIF3D computer code [5] and the second is stochastic model for MONK computer code [2]. The DIF3D computer code solves the multigroup transport equations or approximations of the equations by either nodal or finite difference approaches. It is also the computational engine of the REBUS3 fuel-cycle analysis package [6]. Both the eigenvalue and the external source problems that are pertinent to the GT/AD-MHR system analysis are solved by DIF3D.

The DIF3D-nodal diffusion theory model is used for calculating both the power distributions and reactivity states of the transmuter. A 23 neutron-energy group structure is currently used in the model. This detailed group structure was selected to provide a good representation of the Pu and the Er resonances in the 0.2 to 1.1 eV energy range.

In the DIF3D calculations, 11 rings of hexagonal-prismatic assemblies are modeled, consistently with the GT-MHR transmuter design; this results in 331 radial computational nodes. A radial map of the core is provided in Figure 7. The central location can contain either inner reflector graphite elements or the spallation neutron-source target depending on whether the GT-MHR or AD-MHR is modeled. Similarly, the second ring can contain either inner reflector graphite elements or gas-cooled-fast-TRU assemblies employing fuel particles that have been irradiated for more than four years in the thermal zone. The fourth and fifth rings contain the inner graphite reflectors. The GT-MHR thermal-zone fuel blocks are located in rings six to eight. Rings nine to eleven contain the outer graphite reflector blocks. Axially, the whole length of the active core (793 cm), and additional lower and upper graphite reflector zones (100 cm each), are modeled. Forty axial computational nodes (30 in the TRU blocks) are employed in the DIF3D model. A no-return-current boundary condition is imposed on all external surfaces. It is currently being assumed that the reflector zones contain full density graphite.

The REBUS3 depletion model for the MHR transmuter uses the DIF3D-nodal model discussed above for its neutronics calculations. The 23-group, microscopic

cross sections obtained from the DRAGON unit-element depletion calculations are used for the REBUS3 model. The REBUS3 code capability that permits the fitting of both capture and fission cross sections of the active isotopes is employed in the calculations. This approach approximately accounts for cross section variations due to changes in the neutron spectrum as a function of the depletion. Seventeen heavy-metal nuclides are tracked in the full-core depletion calculations; these are all Pu, Np, Am, Cm and U isotopes. Additionally, 35 fission-product (FP) and one lumped-fission-product nuclides are employed in the REBUS3 model. The 35 FP nuclides account for about 95% of the overall reactivity effect attributable to fission products, and it is expected that this model is more than adequate for the current study. The heavy metal, the FP nuclides, and two erbium isotopes (Er-166 and Er-167) are specified as depletable active isotopes in the REBUS3 model.

The MONK model has explicit modeling for the fuel and burnable poison particles and all the geometrical details of the core as described before. A cylindrical boundary is used for the radial reflector to match the actual configuration shown in Figure 1. The model is shown in Figures 8 and 9. The details of the particle model and TRU assembly are shown in Figures 4 through 6. All the MONK calculations were performed at room temperature except the burnup calculations, which were performed at the average operating temperatures for each material. Also, the MONK burnup analyses used the 172-group nuclear cross section library with the explicit geometrical modeling. The reactivity standard deviation is 0.001 for all the MONK calculations.

Transmuter power distributions predicted by MONK and DIF3D have been compared for a fresh fuel blocks having a heavy metal loading of 787 kg and an Er-167 loading of 27.7 kg. The results indicated that the deterministic approach provides an accurate model of the whole-transmuter. The DIF3D model using block-average cross sections generated by DRAGON gave a maximum assembly power that is different by 0.4% from the MONK value. The maximum difference in block power is 2.5 %.

The results so far obtained in the verification calculations indicate that the deterministic models currently being employed for assessing the GT-MHR design give accurate predictions of core performance parameters when compared to MONK results. Further effort is required to validate the burnup predictions since the deterministic burnup results differ from the MONK results.

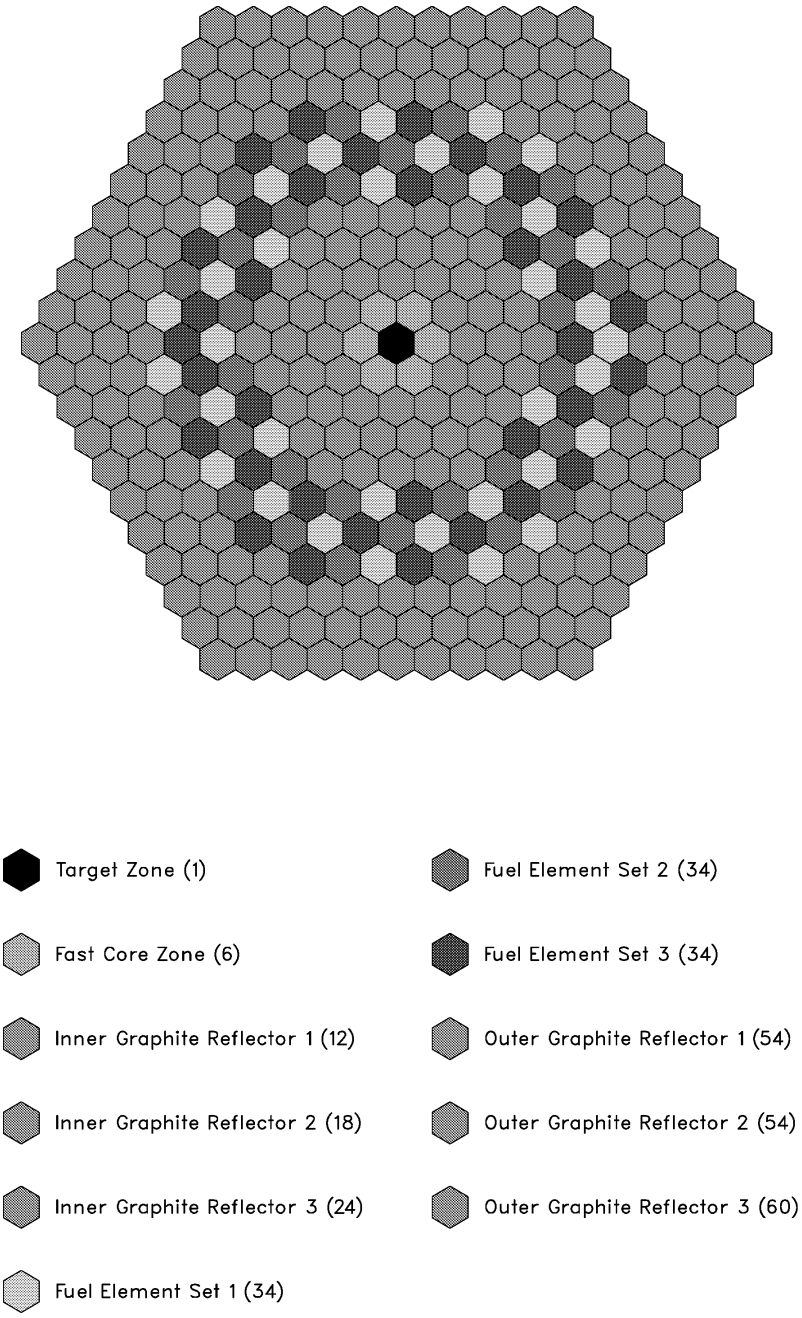

Figure 7. A sample radial core map for the GT/AD-MHR

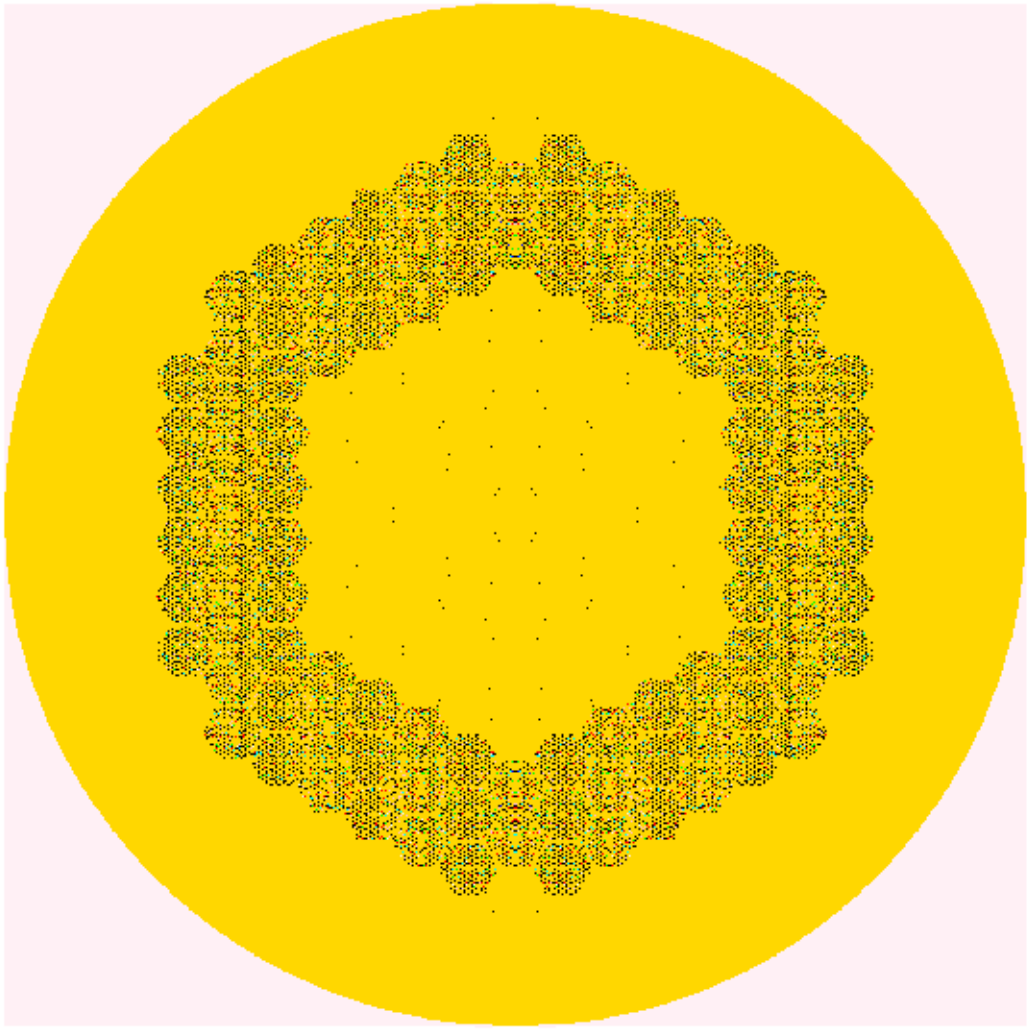

Figure 8. MONK transmuter model

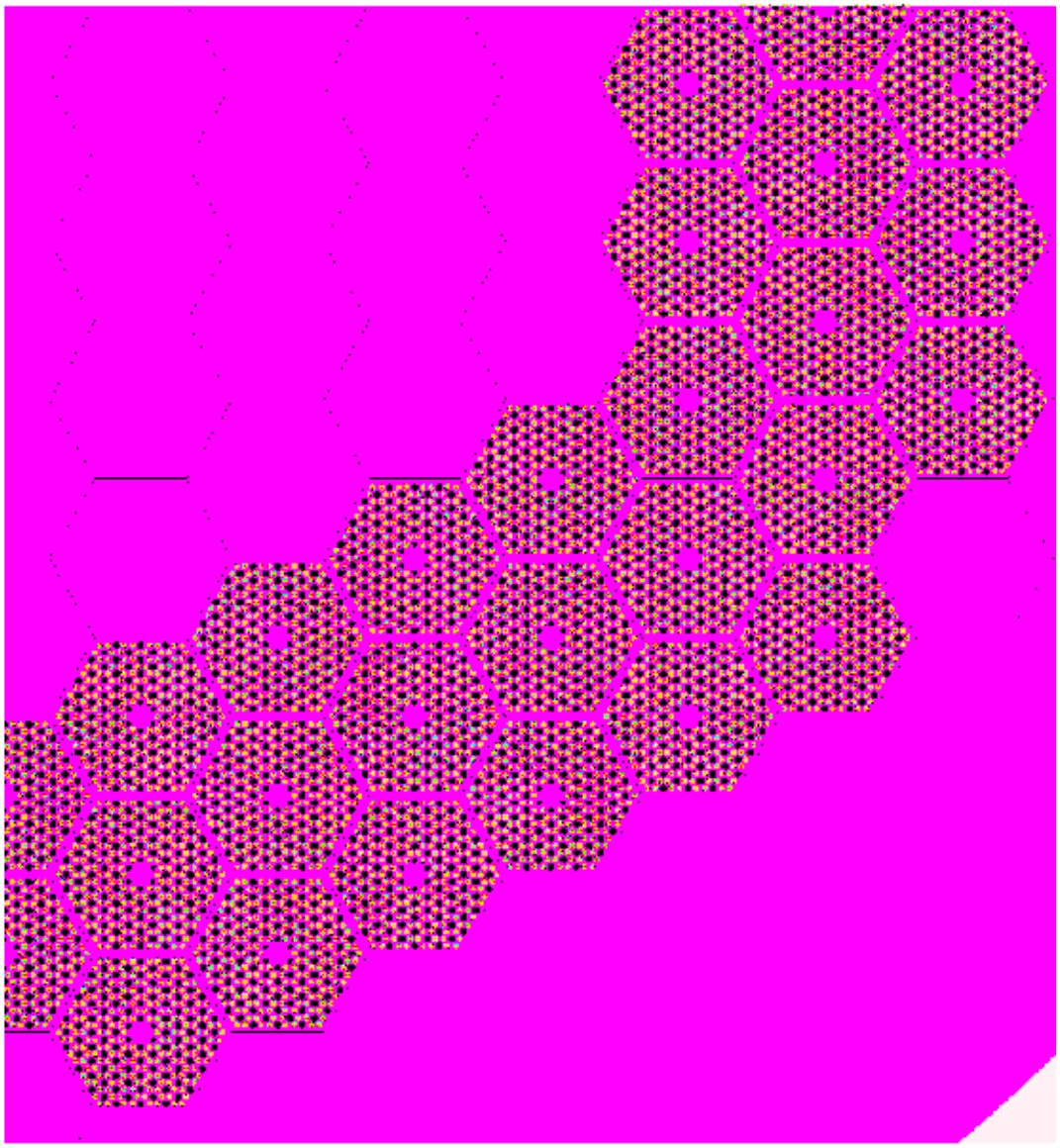

Figure 9. MONK enlarged core section

VI. TRU block parametric studies

Criticality calculations of a TRU block were performed to gain an understanding of the dependence of the block reactivity on erbium loading, fuel kernel diameter, packing fraction, and operating temperature.

The physics of the GT-MHR is complicated by the presence of the low-lying plutonium and Er-167 resonances (0.2-1.1 eV) and by the fact that the neutron spectrum has a low-energy peak about this energy range. This peak can change depending on the transmuter state or material loading. The location of the peak and the direction of the spectral shift greatly affect both the resonance fission and capture rates and dictate the transmuter and block criticality state and the magnitude and sign of reactivity coefficients.

VI.1. Sensitivity to Fuel and Erbium Packing Fractions, and to Particle Size

The DRAGON model has been used to perform some parametric studies of the TRU block in order to obtain an understanding of the variables that affect the block reactivity. Figure 10 shows the variation of the block k_∞ as a function of the fuel-particle packing fraction for three different BP packing fractions, at the normal operating temperature for each material. It should be noted that the blocks considered in the current GT/AD-MHR study have a fuel packing fraction of 0.10 to 0.18. The variation of k_∞ versus the fuel packing fraction shows a peak below 0.05 packing fraction. The shift in the neutron spectrum with the packing fraction is responsible for this trend. As the packing fraction decreases, the carbon-to-heavy-metal ratio increases and leads to an increase in the neutron thermalization causing the neutron spectrum to become softer. This result in fewer neutron captures, which enhances the neutron utilization. The improved utilization of neutrons increases Pu-239 fission rate, which enhances the k_∞ as the fuel packing fraction decreases. The packing fraction corresponding to the highest k_∞ differs for the three curves. As the BP loading increases, the spectrum hardens due to the relative neutron absorption increase in Er-167 and Pu-240. Also, less fuel material is required to achieve the same k_∞. The k_∞ increase with the fuel packing fraction, below the peak value of k_∞, is due to the concentration increase of the fissile elements.

Similar analyses were performed with the MONK block model shown in Figure 4. The fuel-packing factor was varied from 0.05 to 0.25 in the compact at the cooled condition, (room temperature), to define the impact on K_∞ of the block. The MONK analysis used the 172-groups cross section data set. The erbium-packing factor is 0.1. The results show a continuous decrease in K_∞ as the TRU packing factor increases, as displayed in Figure 11. The MONK and the DRAGON results show the same effect on the block reactivity due to the changes in the TRU packing factor.

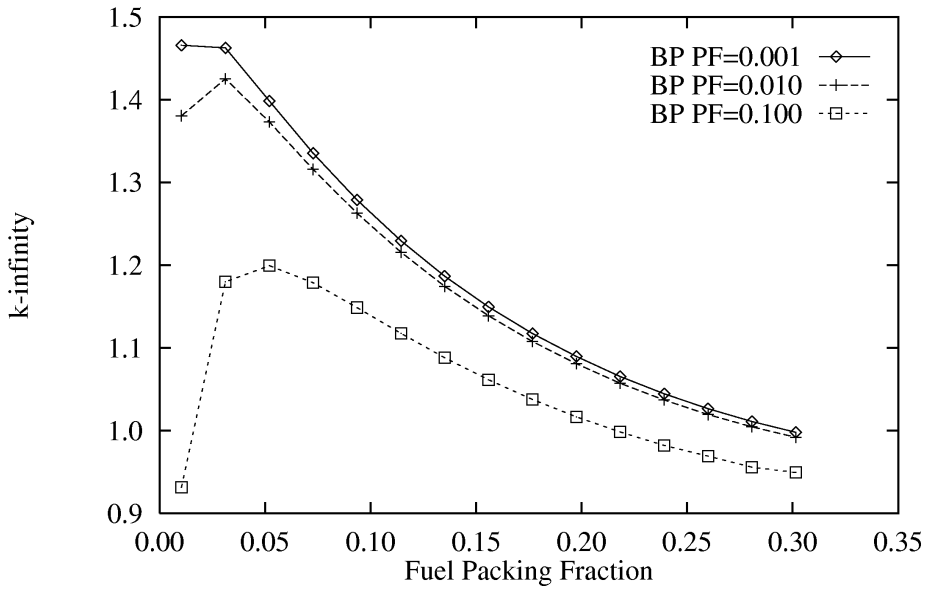

Figure 10. Block k_∞ as a function of TRU packing fraction for different BP packing factors

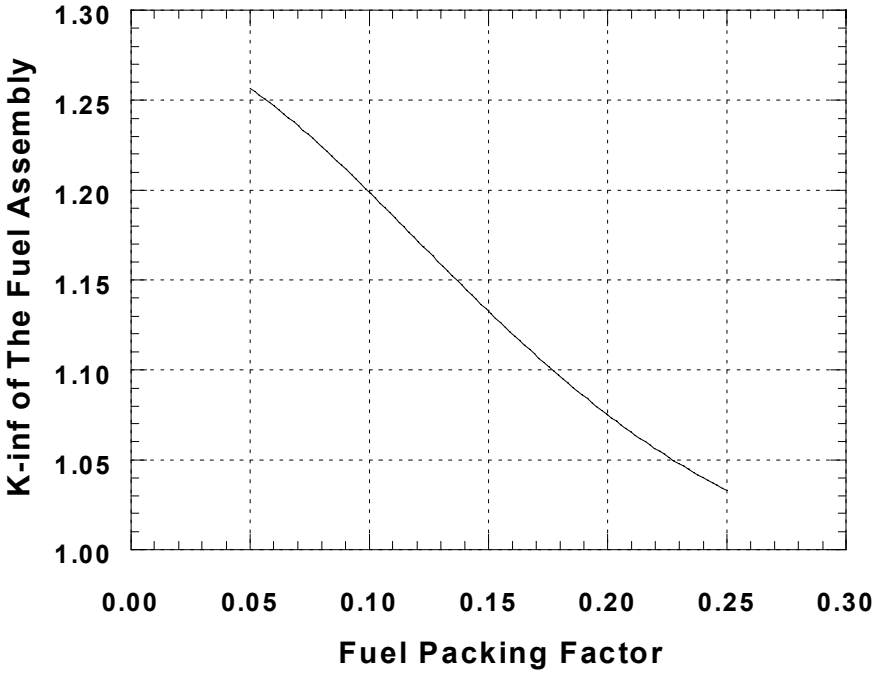

Figure 11. Block k_∞ as function of the TRU packing factor in the compact.

Additional analyses were performed to determine the effect of the fuel kernel size on the block k_∞, for a block with a BP particle packing fraction of 0.10. In these calculations, the thickness of the other particle layers was kept constant. Results for three fuel kernel diameters; base diameter, double the base diameter, and half the base diameter, are displayed in Figure 12. These results were obtained by changing the fuel packing fraction in the same range as that used for generating Figure 10. The results show that for a given heavy-metal mass, the block k_∞ increases as the kernel diameter increases. The increase in the fuel kernel diameter for the same heavy metal mass requires a decrease in the packing fraction and an increase in the distance between kernels. This causes a relative increase in the thermalization of neutrons and produces a softer neutron spectrum. Additionally, the larger kernel diameter increases the self-shielding of the resonance absorbers, particularly Pu-240. Also, the Pu-239 resonance fission cross-section is also reduced by the self-shielding effect. However, the reduction of the Pu-240 absorption cross-section is the predominant effect.

MONK analyses were performed to study the effect of the burnable poison-packing factor on the block K_∞. The burnable poison-packing fraction was varied from 0.05 to 0.40. The analysis used the 172-groups cross section data set and the block model shown in Figure 4. The fuel-packing fraction is 0.1287 in the compact. The results show a continuous decrease in K_∞ as the burnable poison-packing factor increases. The results are displayed in Figure 13.

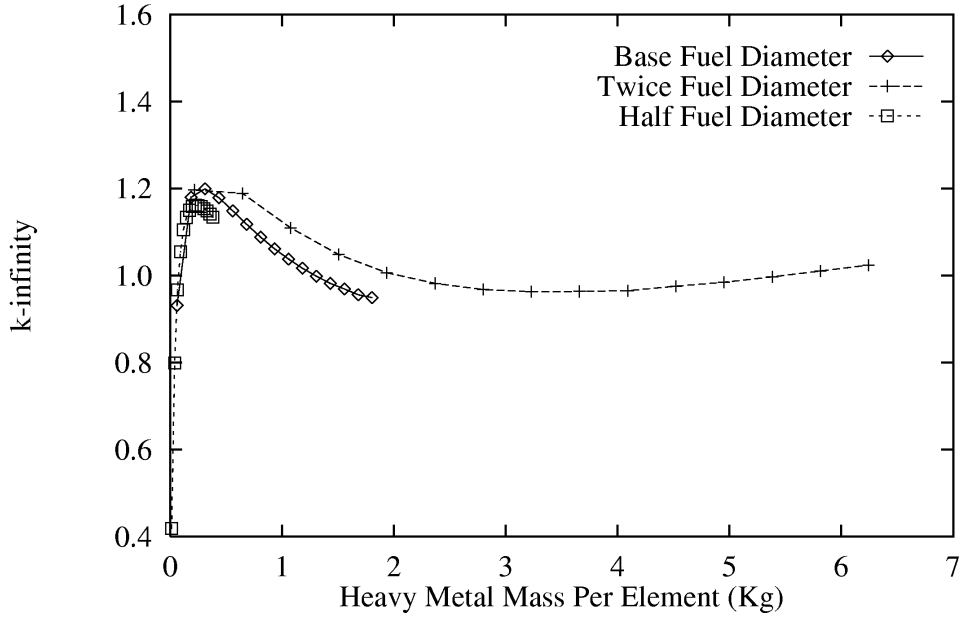

Figure 12. Block k_∞ versus heavy-metal mass with BP PF=0.1

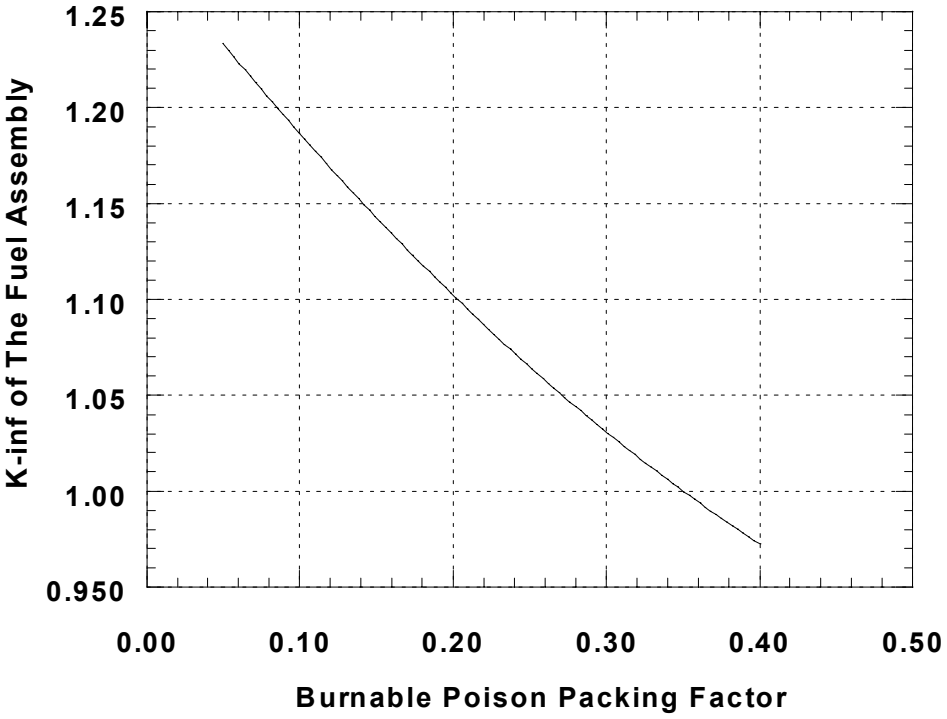

Figure 13. Block k_∞ as function of the burnable poison packing factor in the compact.

VI.2. Sensitivity to Operating Temperatures

One important feature of the GT-MHR core is the net negative temperature coefficient between cold and operating conditions. As the core temperature increases, the neutron spectrum peak shifts toward the absorption resonance of erbium-167. This results in more neutron absorption in the erbium-167. The analysis was performed in steps to define the contribution of each material to this effect. The block model shown in Figure 4 was used for the analysis. The MONK code was utilized to perform the calculation with the 172-groups nuclear data library. Four cases were analyzed as shown in Table IV. The packing fractions are 0.15 and 0.1 for the fuel and the burnable poison, respectively. The first case has all the materials at 293.16 K. In the second case, the fuel particle temperature was changed to the average operating temperature without changing the temperature of the other materials. The third case is similar to the second case with the graphite temperature of the compact changed to average operating temperature. The last case changed the graphite block temperature to the operating temperature. The results from these

cases show that heating the graphite material increases the neutron absorption in erbium-167, which results in a negative temperature coefficient.

Table IV. Temperature effect on k_∞

Material Temperature	K_∞	Relative Difference, %
Cold Conditions	1.1327	--
Hot TRU Particles	1.1112	-1.90
Hot Compact	1.0954	-3.29
Hot Block	1.0562	-6.75

Also, sensitivity calculations performed with the DRAGON computer code indicate that the graphite temperature coefficient is the dominant contributor to the total temperature coefficient of the fresh, unburned TRU compacts. This trend indicates a need for a detailed analysis of the GT-MHR system response to a fast transient, in which the graphite temperature feedback may be slow acting. It was also observed that both the TRU and graphite temperature coefficients become more negative with temperature.

VI.3. Stochastic Burnup Analyses

MONK burnup calculations were performed for the transmuter using the geometrical model shown in Figure 8. In this calculation the TRU compact, graphite block, and the reflector block temperatures are 1043.16, 993.16, and 993.16 K, respectively. The explicit representation of the geometry was maintained in the Monte Carlo and the burnup calculations. The standard deviation for this Monte Carlo calculation is 0.0025. The calculation was performed at constant fission power of 600 MW for 900 days. The packing factors for this configuration are 12.87 and 10% for the TRU and the burnable poison, respectively.

The results show that the fresh transmuter has K-effective of 1.1005. K-effective drops to 1.0 after 600 days. At 900 days, K-effective is about 0.8. About 49% of the TRU are burned in the first 600 days, and 71% are burned at 900 days. At K-effective of 0.9, the burnup is 64%. Er-167 is consumed at much faster rate as shown in Figure 14. Further investigations are required to define the optimum TRU and Er packing factors to achieve 900 days of operation, if it is required, with adequate reactivity and Er-167 concentration for negative temperature coefficient during the critical operating period.

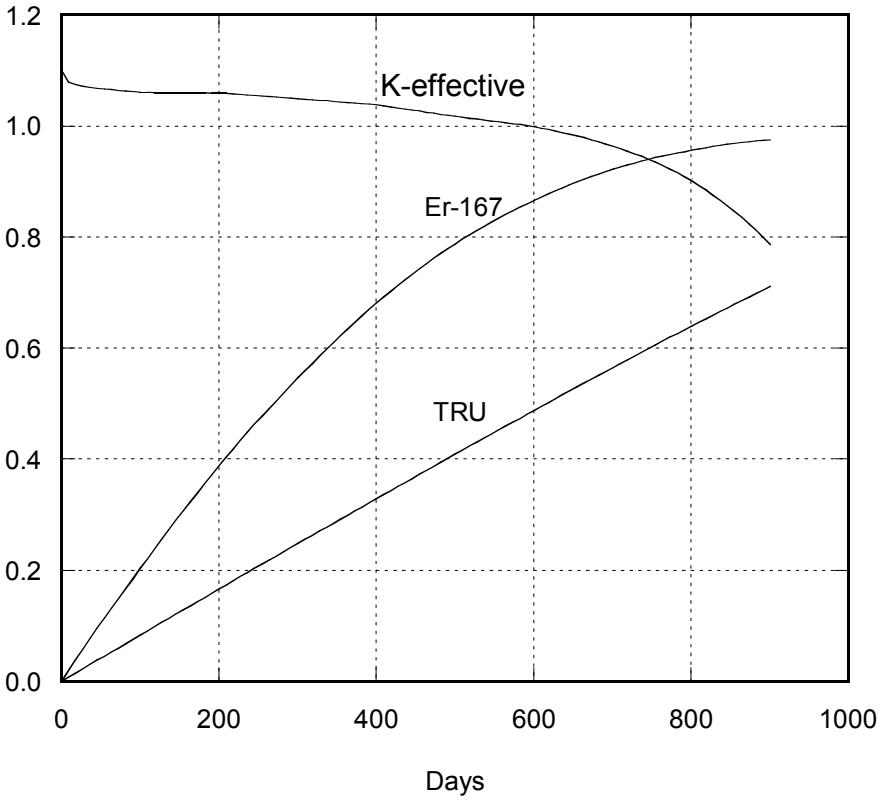

Figure 14. K-effective, TRU-burn fraction, and Er-167 burn fraction as function of the operating time at constant power.

VII. Transmuter Neutronics Parametric Studies

The DIF3D/REBUS3 models were used to evaluate the feasibility of achieving very high Pu-239 and total plutonium consumption rates in the GT-MHR system. Two sets of parametric studies were performed. These calculations were performed without the fast zone in order to gain a better understanding of the GT-MHR transmuter design. The first set of calculations was for the single batch loading scheme, originally proposed with the "Teledial" strategy. These calculations were used to investigate the effect of the initial masses of heavy metal and burnable poison (Er-167) on the design. The second set of calculations was for the three-batch loading scheme. The results of these studies are presented in the following sections. In addition to these calculations a system point design analysis was performed for one of the cases. The results for this latter case are presented in Section VIII.

VII.1. Single-Batch Loading Scheme - Transmuter Studies Without Fast-Zone

Results for the single batch loading scheme without a fast-zone are summarized in Table V. The two design parameters varied in this study are the initial heavy metal and Er-167 masses. The final heavy-metal consumption rate, when k-effective is 0.92 (indicative of the end of residence time in the accelerator-driven system), depends very slightly on the initial masses. The critical cycle length and ITC at the end of the critical cycle are however quite sensitive to these parameters. The effects of variations in these initial masses are discussed in the following subsections.

Table V. Single batch transmuter performance for different TRU and BP masses without fast zone

Parameter	Case							
	0	1	2	3	4	5	6	7
Heavy Metal Loading, Kg	787	1010	1010	1010	1010	1054	600	600
Erbium-167 Loading, Kg	27.73	27.73	13.86	6.93	0.6186	0.6186	0.6186	12.0
Initial k-effective	1.0924	1.0687	1.1046	1.1250	1.1453	1.1382	1.2296	1.1752
Consumption Levels at the end of critical part of the cycle								
Effective Full Power Days	405	450	540	585	585	585	360	333
k-effective	0.9974	0.9988	0.9999	0.9967	1.0012	1.0038	1.0118	1.0121
Pu-239 consumption, %	69	61	70	74	74	72	79	75
Total Pu consumption, %	34	30	36	39	39	37	40	37
Total Heavy Metal Consumption, %	32	27	33	36	36	34	37	34
ITC at 300^{o}C, pcm/^{o}C		-2.16		5.81	6.12	5.11	12.01	10.10
Consumption Levels when k is ~0.92								
Effective Full Power Days	630	855	855	855	855	855	480	467
k-effective	0.919	0.9125	0.9169	0.9189	0.9206	0.9189	0.9078	0.9153
Pu-239 Consumption, %	91	92	92	92	92	92	93	92
Total Pu Consumption, %	54	57	57	57	57	58	53	52
Total Heavy Metal Consumption, %	49	52	52	52	52	53	49	48
ITC at 300^{o}C, pcm/^{o}C		12.84				12.22		
Peak Fast Fluence, 1.0E+21 n/cm^{2}	1.96	2.21	2.54	2.70	2.66	2.67	1.68	1.55

VII.1.1. Initial TRU Mass Influence on the Transmuter Performance

For the same Er-167 mass (case-0 versus case-1 or case-4 versus case-6), the starting k-effective increases as the initial mass of heavy metal decreases. This trend was also observed in the block studies. A lower heavy-metal mass implies a higher carbon-to-plutonium ratio, which enhances neutron thermalization and results in a softer neutron spectrum. A softer spectrum also reduces the resonance absorption in Pu-240 and Er-167 relative to that of Pu-239. These effects increase the fission rate in Pu-239 and hence the k-effective. While the higher k-effective ensures that the system would be critical during operation, it however could be a disadvantage because it indicates a higher excess reactivity, which implies an increase in the control requirements.

A lower initial heavy metal mass gives a higher relative consumption level of plutonium and heavy metal at the end of critical operation cycle (ECOC). The critical operation cycle length is shorter for this case. These can be explained by noting that the fissile mass required to produce a given power is fairly constant, given the similarity in the energy conversion factors. For a given cycle length, the consumption level of heavy metal would be greater in a transmuter with the lower initial heavy metal mass. However, a certain amount of fissile material is required for maintaining criticality, causing the lower heavy metal mass case to reach a k-effective value of unity faster (i.e., shorter cycle length). The rate at which the end of cycle is reached is also affected by the relative absorption of neutrons in fission products, burnable poison, and structural material; which are in turn affected by the neutron spectrum.

One primary disadvantage of the lower initial heavy metal design is the increase in the end of cycle isothermal temperature coefficient in the temperature range below 300^{o}C. The coefficient becomes less negative and reaches a positive value at the end of the cycle as the TRU material decreases during operation. The softer neutron spectrum in the lower mass case is responsible for this behavior. The reduction in neutron capture by Pu-240, Er-167, and the increase in neutron capture by certain fission products explain this result, see additional discussion in the ITC section below.

The ITC becomes more negative as the temperature increases, as shown in Figure 15 for case-5. It has a negative value at the full power operating at an average temperature of about 770^{o}C. The transmuter ITC values were obtained from DIF3D calculations employing 69-group cross sections obtained from DRAGON unit block calculations.

In summary, a longer cycle length is achievable by using a higher heavy metal mass. A higher heavy-metal loading implies a lower specific power per unit mass, which results in a reduction in the consumption level.

VII.1.2. Initial Burnable Poison Mass Influence on the Transmuter Performance

The Pu-239, total plutonium, and heavy metal consumption levels increase as the Er-167 mass decreases (case-1 versus case-4, and case-6 versus case-7). The primary cause of this is the softening of the neutron spectrum as the initial Er-167 mass decreases. The Er-167 loading cannot however be made arbitrarily small because Er-167 provides a strong negative component that help keep the ITC negative (or less positive) at lower temperatures. Additionally, Er-167 is also used to control the initial excess reactivity at the beginning of cycle. The results from case-3 and case-4 are fairly similar because the two cases have a very low Er-167 loading.

VII.1.3. Isothermal Temperature Coefficient (ITC)

The ITC for the recycled LWR-discharge fuel proposed for use in the ATW becomes more positive in the gas-cooled system as the masses of Pu-240 and Er-167 decrease, for low operating temperature range. The decrease of these nuclides occurs with TRU burnup and it is more noticeable for transmuter designs with low initial TRU loading. Typically, the presence of fission products with strong thermal absorption cross sections, e.g., Xe-135 and Sm-149, causes the ITC to go in the positive direction with burnup. Both Er-167 and Pu-240 provide strong negative components to the ITC. An optimum Er-167 loading is therefore required to ensure a negative ITC.

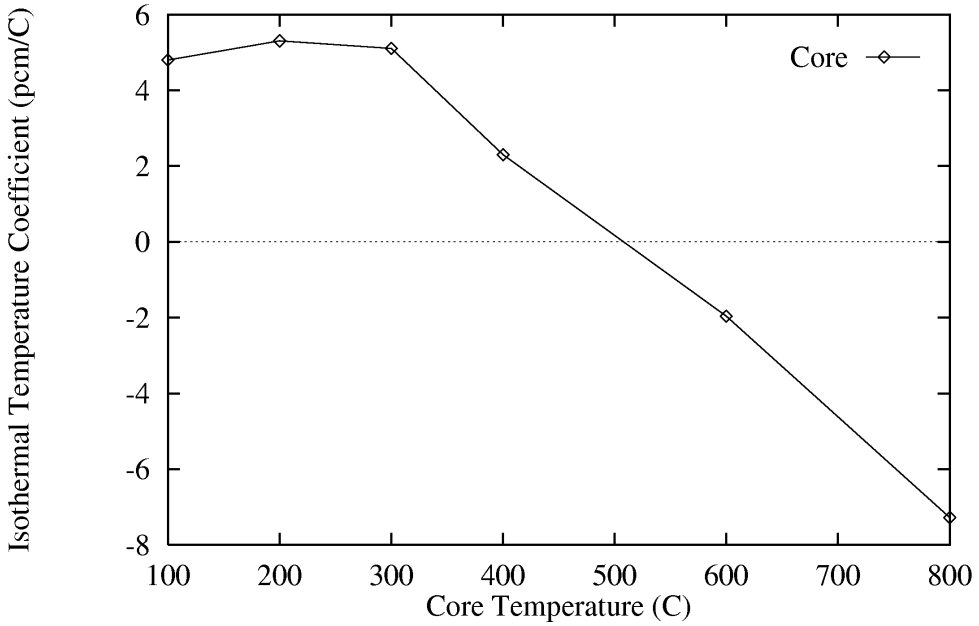

Figure 15 Temperature dependence of ITC for Case-5 at ECOC single batch transmuter

While it is desirable for the ITC to be negative, a positive ITC alone is not an adequate reason to discard a design, particularly, if the prompt Doppler coefficient is sufficiently negative, and the positive ITC occurs in the low temperature range. The ITC becomes more negative as the temperature increases as shown in Figure 15. It has a negative value at full power. This is because the Doppler contribution from Pu-240 increases with temperature.

If it is required to have a negative ITC value over the whole temperature range during the operating cycle, this might be a problem for the single batch scheme. This will require the design to have high heavy metal and Er-167 loadings, which results in low initial k-effective, see for example the initial k-effective of case-1. The initial k-effective decreases as the initial heavy metal and Er-167 masses increase. The transmuter will require the use of a low heavy-metal mass and/or ER-167 loading to get critical system at the beginning of the cycle.

VII.1.4. Fast Neutron Fluence

The peak fast fluence (E > 0.1 MeV) presented in Table V was obtained by finding a representative peak fast flux over the cycle and multiplying it by the discharge cycle length. The peak fluxes for all the cases were fairly similar, typically within 10% of each other. The differences in the peak fast fluence are due primarily to the residence time. These fluence levels are less than the allowable design limit. [1]

VII.2. Three-batch loading scheme - Transmuter studies without fast-zone

Three of the cases studied for a single batch loading scheme were also reevaluated assuming a three-batch loading scheme. The transmuter comprises of three equal sized fuel regions uniformly distributed, and having three different ages of fuel. One segment is discharged at the end of each irradiation cycle, and replaced with a fresh batch. These cases, case-1, case-5, and case-7 represent different combinations of initial heavy metal and Er-167 masses. The results for these cases are summarized on Table VI. Comparing these results to their respective single-batch transmuter results, the excess reactivity, (i.e., the initial k-effective), is smaller for the three-batch transmuter. The transmuter at the beginning of a critical operation cycle (BCOC) state is composed of a mixture of fresh, one-third burn, and two-third burn fuel. Additionally, the fuel discharge length (three times the cycle length of the three batch scheme) is generally larger than the single batch case, and the Pu-239, the total plutonium, and the heavy metal consumption levels are also higher due to the higher discharge burnup.

The general trends observed for the single batch transmuter are still valid for the three batch transmuter. Specifically, as the Er-167 loading increases, the consumption levels and the cycle lengths are greatly reduced. The cycle length is also significantly reduced as the heavy-metal mass is decreased, because of the higher consumption levels as explained before.

Table VI. Three batch transmuter performance for different TRU and BP Masses without fast zone

Parameter	Case		
	1	5	7
Heavy Metal Loading, Kg	1010	1054	600
Erbium-167 Loading, Kg	27.73	0.6186	12.0
Initial k-effective	1.0307	1.0660	1.0911
Cycle Length and Discharge Consumption levels			
Effective Full Power Days	160	260	150
k-effective	1.0062	1.0002	1.0027
Pu-239 Consumption, %	64	86	90
Total Pu Consumption, %	32	50	50
Total Heavy Metal Consumption, %	29	46	46
Peak Fast Fluence, 1.0E+21 n/cm^2	2.36	3.54	2.17
Single Batch Initial k-effective	1.0687	1.1382	1.1752

VIII. System Point Design

In view of the parametric studies described in the previous sections a system point design was developed. The design approach was to maintain the original GA concept as much as possible and to optimize the initial masses of the TRU and erbium. The design uses the three batch scheme to reach a significant cycle length and high burnup.

VIII.1. Transmuter Description

The GA "Teledial" concept aims to run an island containing four transmuters operating concurrently, with three units running in the critical mode, and the fourth running in the accelerator (source) driven mode. It is therefore expected that the cycle length of both the critical and accelerator driven modes would be the same to ensure the operation of all units simultaneously. The preliminary GA proposal specifies a cycle length of one year. Of the cases studied so far case-5 is the only one that meets this requirement, assuming a capacity factor in the range of 0.71 to 0.74. For this reason, case-5 was selected for the system point design (SPD)

analysis. If a single batch scheme is the preferred choice, a higher TRU mass than those studied so far, would be required to get a single-batch cycle length of more than 800 days.

Both the single and three-batch loading schemes with an inner fast zone were analyzed. The nuclide mass flow in the system has been the focus of the current study without the use of explicit fast element design. The fast zone is represented similarly as the thermal zone, using the thermal block dimensions. Nuclide masses representative of the zone composition are used. In the final design, the fast zone elements will have a smaller pitch and different fuel pin dimensions than the thermal zone. The fast elements will use the space vacated by the graphite ring around the target.

Obtaining the initial nuclide masses for the fast zone required several iterations. In the GA proposal, the fuel in the fast-zone is one that has been burned in critical and accelerator driven operations. The critical operation consists of three cycles for the three batch loading scheme or one cycle for the single-batch loading scheme. The accelerator driven operation consists of one-year irradiation driven by the spallation neutrons. The fuel is then additionally burned in the fast zone for another four one-year cycles in the three-batch loading scheme or four-years in the single batch loading scheme. The four years in the latter case is equivalent to one critical operation cycle and one accelerator-driven cycle.

VIII.2. Initial Fast-Zone Nuclide Masses for the Three-Batch Transmuter

The approaches used for getting the initial fuel masses for the fast-zone were dependent on the selected fuel management scheme. For the three-batch transmuter, the following steps were used:

1. A three-batch calculation employing the REBUS3 critical equilibrium cycle model without fast zone, was depleted at a power level of 600 MW. This case was also used to get an estimate of the cycle length. For case-5, the cycle length was found to be about 260 days as shown in Table VI.

2. The homogeneous discharge masses from the end of equilibrium cycle case from step 1, representative of the average thrice-burnt thermal-zone fuel, are used in a REBUS3 non-equilibrium problem. This case was burned at 540 MW for one year, (i.e., 270 full power days) in an accelerator-driven operation. Again no fast-zone is present in this case. The assumption of using uniform masses is sufficiently accurate since it is likely that TRU elements would be both axially and radially shuffled to give a uniform power distribution in the accelerator-driven system. Also the peak-to-average burnup from step 1 is about 1.10 and minimum-to-average is about 0.90.

3. The homogeneous thermal-zone, heavy-metal masses corresponding to the end of the accelerator-driven cycle (EADC), are used in the fast-zone, of a REBUS3

critical non-equilibrium model. Fresh fuel is initially loaded in the thermal zone of this model. This case is burned using a power level of 600 MW. The discharge times of the thermal batches are staggered by one cycle and the fast-zone assemblies reside in the core for three cycles. The procedure it then repeated for five fuel management operations to get an equilibrium state.

4. The homogeneous, fast-zone and thrice-burned thermal-zone masses are retrieved from step 3 and then used in a REBUS3 accelerator-driven non-equilibrium cycle model. The fast-zone and thermal-zone masses remain in their respective positions. The REBUS3 run is made for one cycle using an external source that maintains a power level of 600 MW. It is the fast-zone masses at the end of this cycle that are of interest. Note that in the actual design, the thermal zone masses come from three cycles, they correspond to the ECOC masses. In that case, 2/3 of the TRU has been in storage for two cycles.

5. The process is iterated starting from step 3 until a convergence is achieved.

VIII.3. Initial Fast-Zone Nuclide Masses for the Single Batch Transmuter

The approach used for obtaining the initial heavy-metal masses for the fast-zone of the single-batch transmuter is different from that outlined above. The modified steps for the single-batch transmuter are the following:

1. A single-batch, REBUS3 critical non-equilibrium cycle calculation is carried out for 900 days at a power level of 600 MW without fast zone. This case is also used to get the critical cycle length. For case-5, the cycle length is about 585 days as shown in Table V.

2. The first step is used to get homogeneous masses for both the thermal and fast zones. The homogeneous masses at ECOC, 585 days, are used for the thermal zone. For the fast zone, the homogeneous masses at 810 days are used, which represents an additional 1/3 critical cycle length. These masses are used for a REBUS3 accelerator-driven, non-equilibrium cycle calculation. An external neutron source is used for this calculation at a 600-MW power level for 200 days. An additional load of Er-167 is used in the thermal-zone, to ensure a sub-critical operation.

3. The nuclide masses from the thermal-zone at EADC are obtained from step 2, and they are used in the fast-zone of another REBUS3 critical non-equilibrium cycle. Fresh TRU is loaded in the thermal-zone. This critical cycle is operated at a power level of 600 MW for 720 days to achieve k-effective of about 1.0.

4. The fast-zone and the thermal-zone masses from step 3 are used in a REBUS3 accelerator-driven non-equilibrium cycle calculation. Again, additional Er-167 loading is employed for the thermal zone to ensure a sub-critical operation. The fuel masses is burned for 240 days, about 1/3 of the critical cycle length using

external neutron source at a 600-MW power level. The fast-zone masses at the end of this cycle that are of interest.

5. The procedure is iterated starting from step 3. The thermal zone masses from step 4 are used for the fast zone in step 3. The iterations are carried out until the fast zone masses from step-4 reach convergence.

VIII.4. Discussion of Results

Tables VII and VIII contain the system performance results for the three-batch transmuter employing a fast-zone in both critical and accelerator-driven cycles. The Pu-239, total plutonium and heavy-metal consumption rates at the end of the critical operation cycle (ECOC) and end of the accelerator-driven cycle (EADC) are provided in Table VII. The end-of-cycle discharge masses are provided in Table VIII. The consumption levels are relative to the initially fresh fuel masses. The final consumption levels of interest are those for the fast-zone at EADC. Additionally, the consumption levels at the end of 90 days are provided, which corresponds to the point when k-effective equals 0.9 in the three-batch accelerator-driven cycle. The system k-effective and multiplication factor during the critical operation and accelerator-driven cycles are summarized in Table IX. Similar results are presented for the single-batch transmuter in Tables XI through XII.

Table VII. Three batch transmuter consumption rates in the GT/AD-MHR system

Material	Discharge ECOC	Accelerator-Driven Cycle, After 90 Days		Accelerator-Driven Cycle, EADC (270 Days)	
	Thermal-Zone	Thermal-Zone	Fast-Zone	Thermal-Zone	Fast-Zone
Pu-239, %	86	90	96	95	97
Total Pu, %	50	55	67	63	71
Total Heavy-Metal, %	45	50	61	57	64

Table VIII. Er-167 and heavy metal masses for three batch transmuter

Nuclide		Discharge at End Critical Operating Cycle		Discharge at End of Accelerator-Driven Cycle	
	Initial Mass (Kg)	Thermal Zone Mass (Kg)	Fast Zone Mass (Kg)	Thermal Zone Mass (Kg)	Fast Zone Mass (Kg)
Er-167	0.61	------	0.00	0.00	0.0
Np-237	43.20	25.52	18.54	20.41	14.91
Pu-238	12.65	46.07	56.52	49.33	52.94
Pu-239	543.21	74.68	22.79	27.13	17.08
Pu-240	251.64	133.47	73.95	84.81	63.50
Pu-241	84.20	134.50	63.96	85.42	44.41
Pu-242	52.69	86.21	107.35	104.39	98.67
Am-241	52.69	19.05	17.60	11.15	13.10
Am-242	1.05	0.46	0.26	0.24	0.26
Am-243	10.53	29.45	37.52	35.34	43.06
Cm-242	0.00	7.83	0.60	7.15	3.00
Cm-243	0.00	0.26	0.17	0.21	0.18
Cm-244	2.11	15.61	21.28	22.29	24.31
Cm-245	0.00	1.53	2.78	1.53	6.18
Total Heavy-Metal Mass	1054.00	574.60	423.42	449.40	381.60

Table IX. Three batch transmuter, k-effective, multiplication factor and power sharing

Critical Operation Cycle			
Burn Time (Days)	k-effective	Power Fraction	
		Thermal Zone	Fast Zone
0	1.074	0.97	0.03
135	1.030	0.97	0.03
270	1.006	0.97	0.03
Accelerator-Driven Cycle			
Burn Time (Days)	Multiplication Factor	Power Fraction	
		Thermal Zone	Fast Zone
0	0.963	0.90	0.10
90	0.896	0.81	0.19
180	0.817	0.70	0.30
270	0.732	0.59	0.41

Table X. Single batch transmuter consumption rates in the GT/AD-MHR system

Nuclide	Discharge ECOC	Accelerator-Driven Cycle, EADC (240 Days)	
	Thermal-Zone	Thermal-Zone	Fast Zone
Pu-239, %	80	91	94
Total Pu, %	44	56	61
Total Heavy-Metal, %	40	51	56

Table XI. Er-167 and heavy metal masses for single batch transmuter

Nuclide		Discharge at End Critical Operating Cycle		Discharge at End of Accelerator-Driven Cycle	
	Initial Mass (Kg)	Thermal Zone Mass (Kg)	Fast Zone Mass (Kg)	Thermal Zone Mass (Kg)	Fast Zone Mass (Kg)
Er-167	0.61	0.09	0.00	2.29	0.0
Np-237	43.20	27.58	22.07	23.02	19.16
Pu-238	12.65	40.60	52.53	46.22	51.58
Pu-239	543.21	106.60	42.81	47.78	33.36
Pu-240	251.64	173.42	133.45	134.81	122.56
Pu-241	84.20	129.29	81.48	97.77	66.57
Pu-242	52.69	79.63	93.62	93.33	90.32
Am-241	52.69	21.31	21.22	14.53	18.50
Am-242	1.05	0.54	0.34	0.31	0.38
Am-243	10.53	26.26	32.86	31.40	36.99
Cm-242	0.00	9.13	0.91	7.72	2.66
Cm-243	0.00	0.23	0.24	0.26	0.23
Cm-244	2.11	11.62	14.68	15.74	15.31
Cm-245	0.00	2.24	3.65	2.73	6.58
Total Heavy-Metal Mass	1054.0	628.50	499.9	515.68	464.29

The following main observations are obtained from the results given in Tables VII to XII:

1. The consumption levels at the end of the critical operation cycles of the single-batch and three-batch transmuter with the fast-zone are similar to those presented on Tables V and VI for the same transmuters without the fast-zones. The relatively larger differences for the single-batch transmuter results because of the much longer cycle length for the case with the fast zone.

   The reactivity trends of the critical operation cycle are also similar to the trends obtained for the cases without fast-zones. Specifically, the three-batch transmuter

has a lower excess reactivity at BCOC and higher plutonium and heavy-metal consumption levels at the ECOC.

Table XII. Single batch transmuter, k-effective, multiplication factor and power sharing

Critical Operation Cycle			
Burn Time (Days)	k-effective	Power Fraction	
		Thermal Zone	Fast Zone
0	1.137	0.96	0.04
80	1.100	0.96	0.04
240	1.079	0.96	0.04
480	1.042	0.96	0.04
720	0.991	0.95	0.05
Accelerator-Driven Cycle			
Burn Time (Days)	Multiplication Factor	Power Fraction	
		Thermal Zone	Fast Zone
0	0.963	0.87	0.13
80	0.927	0.80	0.20
160	0.880	0.72	0.28
240	0.827	0.64	0.36

2. The multiplication factor of the three-batch transmuter varies from 0.963 to 0.732, implying a seven-fold increase in the source strength over the cycle, to keep the power level constant. A five-fold increase is required for the single-batch transmuter. Limitations on the maximum source level might restrict the cycle length for these cases. In that event, there could be a mismatch between the cycle lengths of the critical operation and the accelerator-driven cycles that could complicate the “Teledial” concept.
   The single-batch and three-batch transmuters have the same multiplication factor of 0.963 at the beginning of the accelerator-driven cycle. The EADC multiplication factor of the three-batch transmuter falls off drastically over the cycle relative to that of the single-batch transmuter, 0.73 versus 0.83. This is because the initial reactivity of the single-batch transmuter is much higher than that of the three-batch transmuter, this initial reactivity is suppressed using additional burnable poison particles.

The multiplication factor at the end of the accelerator part of cycle (0.73 or 0.83) is lower than the permitted value in actual operation. This low value would require a high beam power and it would make the accelerator cost prohibitive. The low multiplication factors resulted because the sub-critical mode of cycle length was set to that of the critical mode.

3. The power fractions of the fast and thermal zones are fairly constant during the critical operation cycle in both single-batch and three-batch transmuters. The fast-zone accounts for about 3 to 5% of the total power in both the single-batch and three-batch transmuters.

   The power fraction of the fast–zone increases with burnup in the accelerator-driven cycle, for both the single-batch and three-batch transmuters. This is because the neutron flux falls off with increase in distance from the source, attenuated by the material properties of the zones along the path. As the system becomes more subcritical, and as the neutron multiplication in the thermal-zone decreases with burnup, a more pronounced tilt results.

   The transmuter radial power distributions are presented on Figures 16 and 17, for the three-batch transmuter and Figures 18 and 19 for the single-batch transmuter. The axial power profiles in the fast-zone of the critical operation and in the accelerator-driven cycles are also displayed in Figures 20 and 11. The radial and axial power profiles are normalized to the transmuter average power density. The critical operation power distributions are relatively flat and the peak is within acceptable limits. The power peaking is more pronounced in the accelerator-driven cycle than in the critical operation cycle. The highest power densities are recorded in the fast-zone of the accelerator-driven cycle, and they increase with irradiation time. The axial power profile of the fast-zone peaks significantly at the center where the external source is located.

4. Because the fast zone has about 3 to 4% of the total power during the critical part of the fuel cycle, the plutonium and heavy-metal consumption rates of the fuel residing in this zone is quite small. Additionally, the fast zone has about 24 to 25% of the total power during its stay in the accelerator-driven part of the fuel cycle therefore the overall consumption of TRU in this zone is relatively small.

5. A harder neutron spectrum exists in the fast zone relative to the thermal zone, as shown in Figure 22 for the three-batch transmuter. The fast-zone spectrum is softer than that possible in a fast transmuter without thermal zone. Figure 23 shows the fast zone neutron spectrum at the beginning of accelerator-driven cycle with a zero current boundary condition.

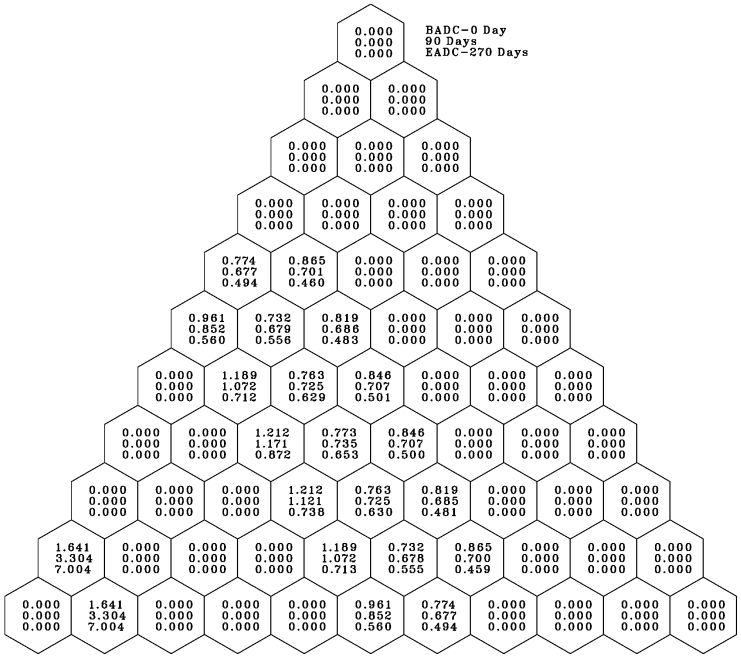

Figure 16. Sixth-transmuter radial power distribution for three-batch critical operation cycle, the core central location at lower left hexagon

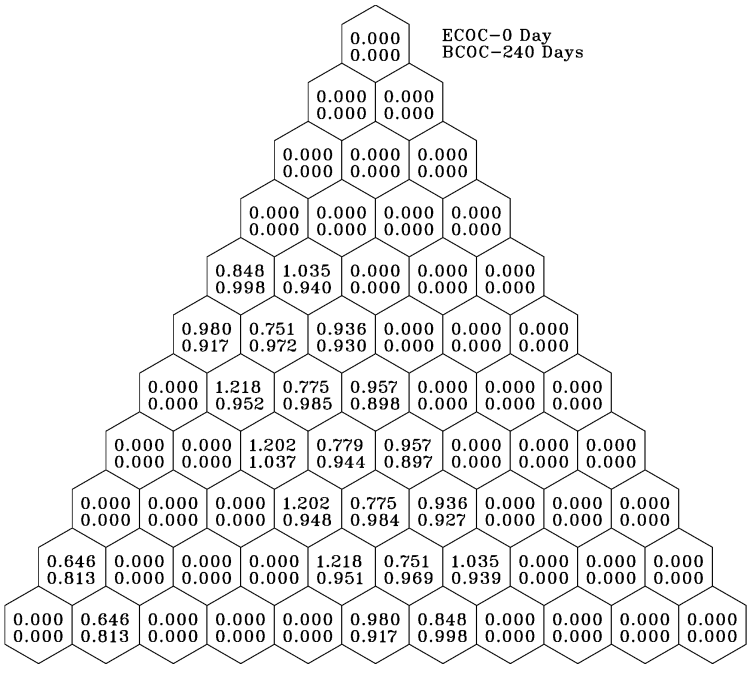

Figure 17. Sixth-transmuter power distribution for three-batch accelerator-driven cycle, the core central location at lower left hexagon

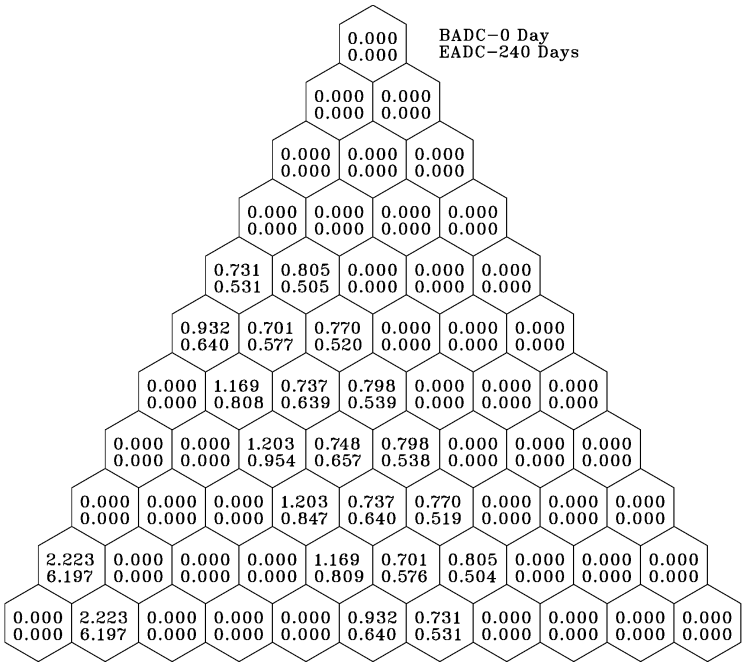

Figure 18. Sixth-transmuter radial power distribution for single-batch critical cycle, the core central location at lower left hexagon

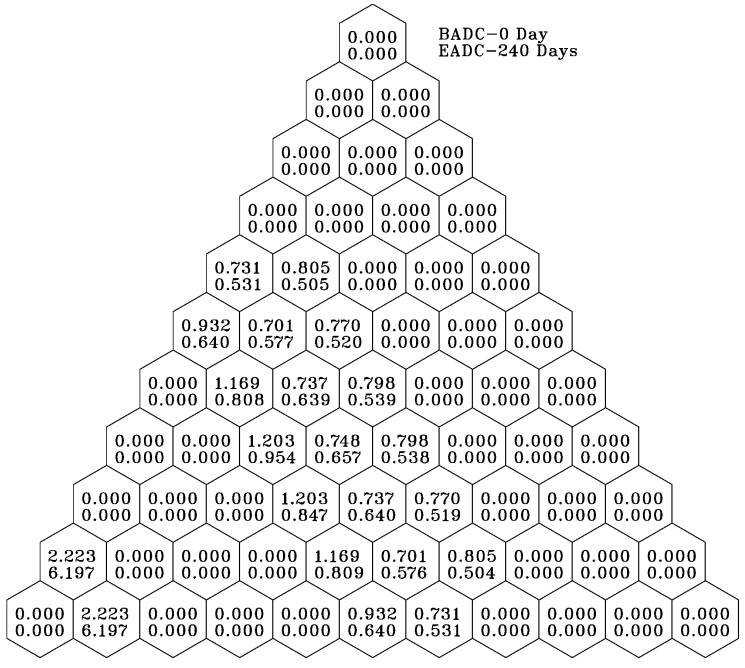

Figure 19 Sixth-transmuter power distribution for single-batch accelerator-driven cycle, the core central location at lower left hexagon

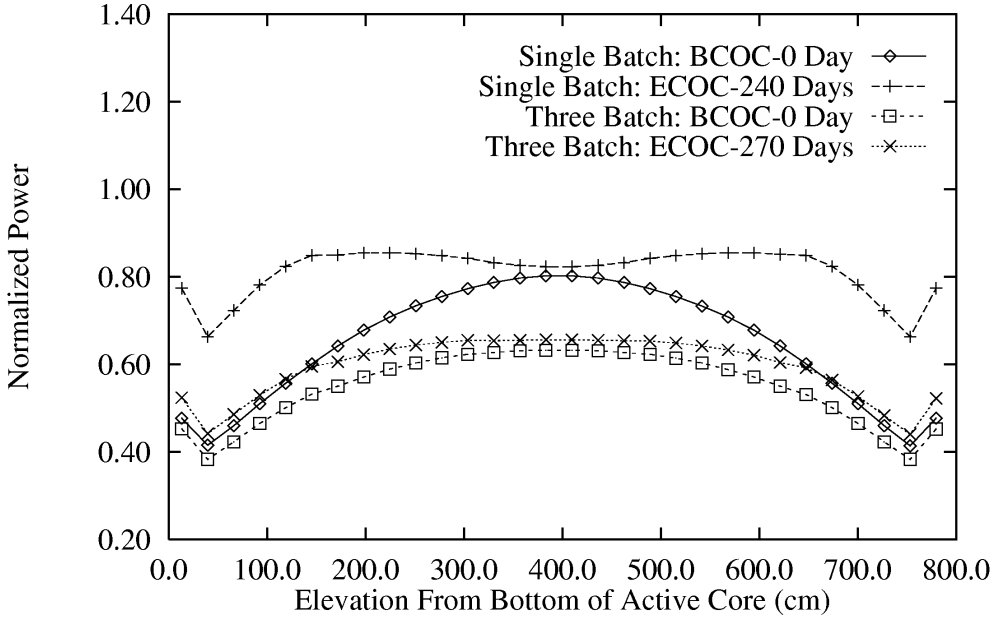

Figure 20. Axial power distribution in the fast-Zone during the critical cycle

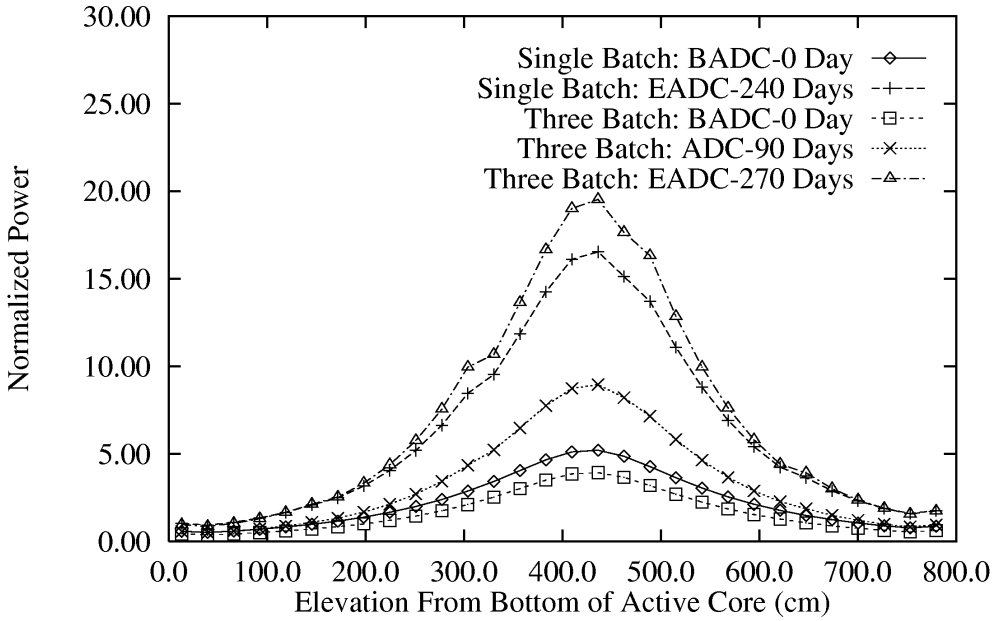

Figure 21. Axial power distribution in the fast-zone during accelerator-driven cycle

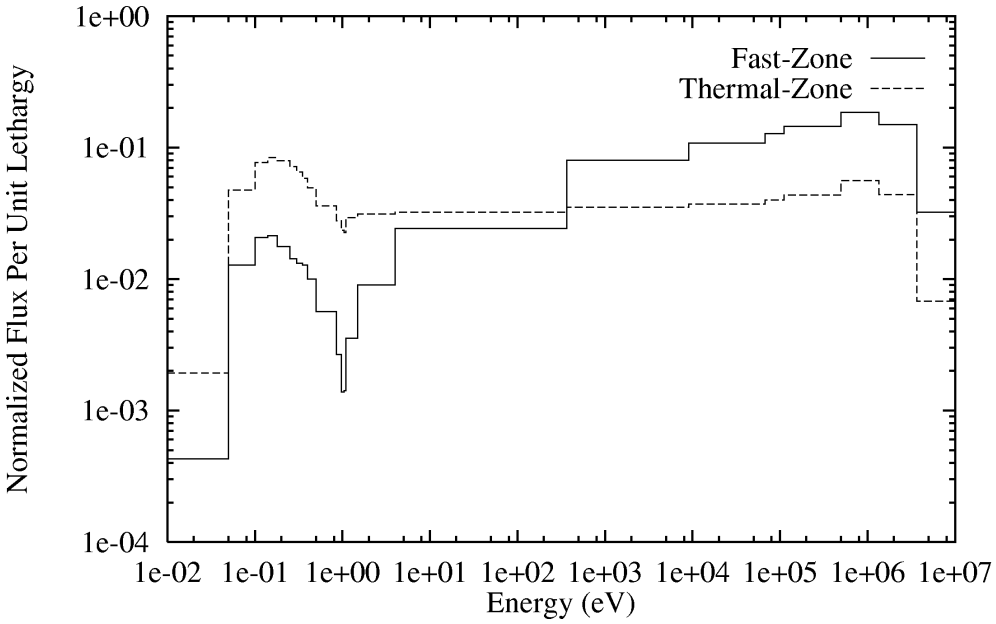

Figure 22. Zonal spectra at the beginning of the accelerator-driven cycle for the three-batch transmuter.

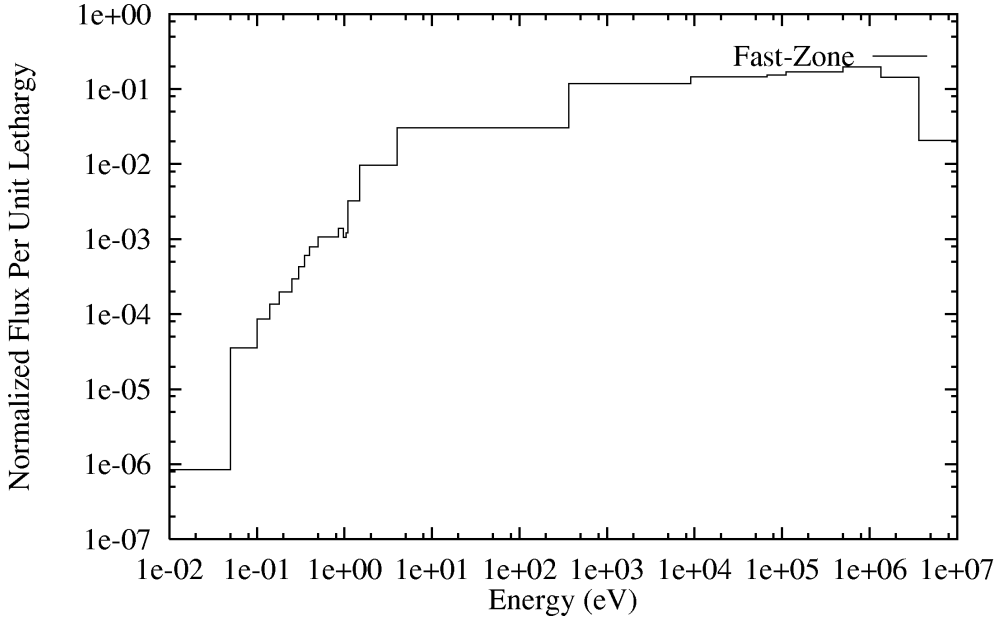

Figure 23. Fast-zone critical spectrum at the beginning of accelerator-driven cycle composition for the three-batch transmuter with a zero current boundary condition.

IX. Preliminary Thermal Hydraulic Analysis of the Fast Region

An estimate of the allowable power density in the fast spectrum zone of the ATW/GT-MHR conceptual design is made based on the thermal-hydraulic characteristics of: 1) the proposed Gas Cooled Fast Reactor (GCFR) design, and 2) the proposed GT-MHR design. Table XIII compares the performance characteristics of these reactor designs. The GCFR design data were taken from Reference 7, and the GT-MHR design data were taken from Reference 8.

The fast spectrum zone of the ATW/GT-MHR is assumed to consist of an array of hexagonal GCFR assemblies, made up of fuel pins clad with stainless steel arranged on a triangular mesh. For reference, the cladding outer diameter, pin pitch, and pin length are assumed to be identical to the GCFR design.

The power density in the fast zone will be limited by the available coolant flow rate provided by the core pressure drop in the GT-MHR design. According to the information presented in Table XIII, the core pressure drop available in the GT-MHR design is 0.051 MPa. In contrast, an average GCFR core subassembly, operating at a power density of 120 W/cc, was cooled by a pressure drop of 0.29 MPa. The axial distribution of the GCFR pressure drop is indicated in Table XIV, which was taken from Reference 7. Note that 44% of the GCFR subassembly pressure drop occurs in the active core region, in which the cladding surface has been roughened to enhance heat transfer. If the GCFR assembly was to be cooled by a 0.051 MPa coolant pressure drop, then assuming the pressure drop is approximately proportional to the square of the flow rate, the new flow rate is $(0.051/0.29)^{1/2}$ = 42% of the original GCFR flow rate, if all other factors remain fixed. Thus, the ATW/GT-MHR pressure drop would provide 42% of the heat removal capability of the GCFR design, if the subassembly hydraulic characteristics, flow area, hydraulic diameter, length, remained the same.

A second consideration is the coolant pressure, which determines the value of the cladding-to-coolant heat transfer coefficient. Note that the GT-MHR operates at a pressure of about 7 MPa, compared to the GCFR pressure of about 10 MPa. The heat transfer coefficient is proportional to the 0.8 power of the Reynolds number, which is directly proportional to the density, and hence to the pressure through the ideal gas law. So the heat transfer coefficient is approximately proportional to the 0.8 power of the pressure. Taking the lower GT-MHR pressure into account reduces the GCFR heat removal by a factor of $(7.0/10.0)^{0.8}$ = 75%.

Consideration must also be given to changes in the hydraulic characteristics of the GCFR subassembly design. The overall GCFR subassembly length is 490 cm, considerably shorter than the GT-MHR core height of 793 cm. Extension of the GCFR pin length would increase the friction pressure drop in direct proportion to the length increase, and reduce the heat removal capability accordingly.

Assuming that the fast region has a volume equivalent to that of six standard TRU block columns, it can accommodate, by comparison to the GCFR characteristics, an

average power density such that the total power of the fast region is roughly 26% of the total core power.

Table XIII. Comparison of reactor design characteristics

	GCFR	GT-MHR
Core Power, MW	1088	600
Coolant Pressure, MPa	10.5	7.07
Core ΔP, MPa	0.29	0.051
P_{avg}, W/cc	120.	6.6
P_{peak}, W/cc	180.	-
Core ΔT_{avg}, ^{o}C	232	360
Core Height, cm	120	793
He Flow, kg/s	949	320

Table XIV. Pressure drop in various parts of the GCFR fuel subassembly.

	% P	Length, cm
Inlet	8.3	-
Lower Axial Blanket	4.8	60
Core Region (Roughened Cladding)	44.0	120
Upper Axial Blanket	7.0	60
Spacers	22.6	-
Acceleration	2.1	-
Outlet	11.2	-

X. Required future R&D activities

The point design described in this report achieves very high plutonium burnups and limited minor actinides burnups. Also, the studies of this report were very preliminary and several potential issues discussed in the following sections need to be addressed:

X.1. Neutronics optimization

While high burnups have been calculated for the discharge TRU, it was also observed that the final burning stage in the fast region was not very effective due to the relatively soft spectrum in the central fast region. This softening is due to the return of moderated neutrons from the graphite reflector between the thermal and the fast zone. Adding thermal absorbers, e.g. boron, cadmium, or certain long-lived fission products, in the graphite reflector around the fast region, could probably minimize these low energy neutrons. Nevertheless, this would not increase the fast flux in the central region, necessary for effective transmutation of the higher minor actinides but it reduces the thermal fission reaction rate and the power density in the fast zone. More efficient solutions have been under consideration. One simple solution is to adopt a double strata system, where a thermal, accelerator driven or not, gas cooled transmuter would be used to burn as much plutonium as possible. Then, the TRU would be reconstituted using an intermediate reprocessing step and introduced into a fast accelerator driven transmuter for deep burning of the minor actinides. Separation of the fast and thermal burning functions, while less elegant than the proposed GA approach, might avoid complex engineering issues. Another solution is to redesign the fast region within the proposed concept to make it a better neutron multiplier, thus generating its own sustained fast flux; this could be achieved by enlarging it and providing it with more fissile materials.

Several paths have been identified for increasing the performance of the thermal region. For example, lower TRU inventories and larger particle sizes might result in deeper burnups, though the resulting shorter cycle lengths and potential power peaking might be operational issues. Also, larger transmuter outer diameters might result in higher performances, but at the cost of having to significantly improve the shielding characteristics of the outer reflector.

Control issues will need to be addressed and control methods require development for the initial excess reactivity, the transmuter reactivity control, and the accelerator beam intensity during the subcritical stage. As much as possible, it is desirable to obtain a flat reactivity profile during operations, in order to avoid excessive power peaking. This would give the preference to transmuters with large fissile inventories and elaborate TRU management schemes, for example, a long life transmuter with several TRU batches.

No attempt has yet been made to find suitable modes for incinerating Long Lived Fission Products (LLFP). Positions in the inner or outer reflector seem ideally suited for these tasks. Burning rates will need to be estimated and LLFP target design will need to be developed.

X.2. Heat removal

Heat removal of the thermal and fast regions have been studied in a preliminary manner. For the thermal region, comparison of calculated average and peak power

densities to those calculated for HTGR indicates that the thermal region of the transmuter is probably satisfactory with respect to the heat removal. This needs further verification by adequate calculations once a preliminary design has been developed.

Heat removal from the fast region seems to be feasible, on average, but there is a serious danger of reaching very high peak power values close to the target. This region of the core seems particularly sensitive to the design parameters, which requires iteration between the transmuter design and the target design. It should be noted that at this point, no design exists for either of these two components.

X.3. Safety

The original designs of the GT-MHR have achieved high levels of passive safety through the use of the TRISO coated fuel and the introduction of large masses of graphite, which provide significant thermal inertia. The GT/AD-MHR has different design features that require a new safety assessment. For example, the fast region has significantly lower thermal inertia, which requires creative means to either increase the thermal inertia (e.g. addition of matrix material in the TRU) or create heat conduction paths designed in the TRU subassembly to dissipate heat during transient conditions.

Another important design issue is the relatively large positive temperature coefficient observed at cold temperatures, as shown in Figure 15. While it is not clear that there is a safety risk associated with that behavior, this issue needs to be addressed. Other neutronics design options can be utilized to reduce this positive value including the addition of erbium burnable poison and the use of multiple TRU batches.

X.4. Fuel behavior

While the TRISO coated particles have been extensively tested in the past, they have never achieved the very high burnup required for the ATW program. The highest burnup achieved for Pu bearing fuels is 80 % [9]. Furthermore, there is no experience fabricating TRISO coated particles with significant minor actinide contents. Fabrication problems might occur, for example the americium volatility needs to be accommodated in the fabrication procedure.

The reconstitution procedure of the fuel into a fast assembly needs to be investigated. In particular, it is not clear whether the irradiated compacts can be integrally transferred to the fast region, which causes excessive neutron thermalization. In that case, the fuel particles would need to be separated from the graphite matrix, and recast into a form suitable for transmuting in the fast assembly.

The fast assemblies and the fast region need to be designed to maintain a fast neutron spectrum, while insuring adequate heat removal capability during normal and abnormal conditions. Methods to achieve a fast neutron spectrum have been discussed above. Heat removal during normal operations requires designing the assemblies with enhanced cooling features, such as roughened or ribbed cladding and adequate coolant parameters for acceptable operating performance. Abnormal conditions need to be studied to insure passive safety performance. As mentioned before, the addition of inert material to the fuel would increase its thermal inertia, the use of thermal bridges would help conducting the decay heat during abnormal operating conditions.

In the current studies, it was assumed that the fuel would withstand the very high-calculated burnups. Nevertheless, if the fuel particles performance could not be demonstrated up to these levels an intermediate-reprocessing step, probably between the thermal and fast irradiation steps would need to be devised. This would imply separating the TRISO particles from the graphite binder; mechanically or otherwise breaching the silicon carbide protective coating; dissolving and recuperating the TRU contents; and reforming a new fuel form.

The design of LLFP bearing elements needs to be assessed for selecting the most appropriate form. The selected form requires development and testing.

X.5. Target design

The current system design leads to excessive power peaking in the fast region. This is due to the peaked neutron source used in the calculation, and the very low k_{eff} reached at the end of the subcritical cycle. Two R&D actions are required to alleviate this potential problem:

- The system design should be optimized to keep a relatively high k-effective at the end of the subcritical cycle.
- The target and fast region designs need to be performed with the objective of spreading the source as much as possible.

X.6. System design

The preliminary studies performed for this document have been constrained by the desire to maintain the design and operating conditions of the GT-MHR. There is no guarantee that these dimensions and operating conditions are optimal for the mission of burning transuranic waste. Global system optimization studies are needed to achieve this goal.

REFERENCES

1. Private Communications, General Atomics, March 2000.

2. The ANSWERS Software Package, MONK - A Monte Carlo Program for Nuclear Criticality Safety and Reactor Physics Analyses, User Guide for Version 8, ANSWERS/MONK(98)6, AEA Technology, UK.

3. Y. Gohar, T. A. Taiwo, and P. J. Finck, "Neutronics Analyses of the General Atomics Accelerator Transmutation of Waste Concept Based on the Gas-Turbine-Modular Helium Cooled Reactor Technology," ANL/TD/TM01-17, Argonne National Laboratory, (2001)

4. G. MARLEAU et al., "A User's Guide for DRAGON," IGE-174, Rev. 3, Ecole Polytechnique de Montreal (Dec. 1997).

5. K. L. DERSTINE, "DIF3D: A Code to Solve One-, Two-, and Three-Dimensional Diffusion Theory Problems," ANL-82-64, Argonne National Laboratory, (1984).

6. W. S. Yang and H. Khalil, "Analysis of the ATW Fuel Cycle Using the REBUS-3 Code System," *Trans. Am. Nucl. Soc.,* 81, 277 (1999).

7. E. Waltar and A. B. Reynolds, Fast Breeder Reactors, Pergamon Press, 1981.

8. T. W. Chan, R. D. Pfremmer, and V. Tangirala, "Preliminary Transient Analyses of Gas Turbine Modular Helium Reactor (GT-MHR)," Proceedings of the International Topical Meeting on Advanced Reactors Safety, American Nuclear Society, Pittsburgh, Pennsylvania, April 17-21, 1994.

9. M. Miller and W.J. Scheffel, "Postirradiation Examination and Evaluation of Peach Bottom FTE-3," GA-906939, November 1975.

DISTRIBUTION LIST FOR ANL/TD/TM01-16

Internal

R.K. Ahluwalia
S.K. Bhattacharyya
M. Billone
J. Brooks
J. Cahalan (5)
Y. Chang
D. Crawford
D. Ehst
P. Finck (10)
E. Fujita
Y. Gohar (10)
D. Hill
R. Hill
H. Khalil
J. Laidler
J. Liaw
S. Majumdar
V. Maroni
R. Mattas
K. Natesan
B. Picologlou
C. Reed
D.L. Smith
T. Taiwo (5)
R. Valentin
D. Wade
R.W. Weeks
T. Yule
TIS

External

ANL-E Library
ANL-W Library
DOE/OSTI
J. Anderson, Los Alamos National Laboratory, Los Alamos, NM
E. Arther, Los Alamos National Laboratory, Los Alamos, NM
C. Baker, University of California, San Diego, CA
D. Baldwin, General Atomic, San Diego, CA
C.G. Bathke, Los Alamos National Laboratory, Los Alamos, NM
A. Baxter, General Atomics, San Diego, CA
D.R. Bennett, Los Alamos National Laboratory, Los Alamos, NM
S. Berk, U.S. Department of Energy, Germantown, MD
E.E. Bloom, Oak Ridge National Laboratory, Oak Ridge, TN
C. Bolton, U.S. Department of Energy, Germantown, MD
M. Cappiello, Los Alamos National Laboratory, Los Alamos, NM
E. Cheng, TSI Research Inc., San Diego, CA
V. Chernov, Bochvar Research Institute of Inorganic Materials, Moscow, Russia
R. Conn, University of California, San Diego, CA
R. Dagazian, U.S. Department of Energy, Germantown, MD
W. Dove, U.S. Department of Energy, Germantown, MD
M. Eid, CEA, Gif-sur-Yvette, France
L. El-Guebaly, University of Wisconsin, Madison, WI
G. Emmert, University of Wisconsin, Madison, WI
O. Filatov, Efremov Scientific Research Institute, St. Petersburg, Russia
U. Fischer, Forschungszentrum Karlsruhe, Germany
M. Fuetterer, CEA, Gif-sur-Yvette, France
M. Gasparotto, ENEA, Frascati, Italy

L. Giancarli, CEA, Gif-sur-Yvette, France
F. Goldner, Department of Energy, Germantown, MD
R. Goldston, Princeton Plasma Physics Laboratory, Princeton, NJ
J. Gulliford, AEA Technology, United Kingdom
W.G. Halsely, Los Alamos National Laboratory, Los Alamos, NM
R.A. Krakowski, Los Alamos National Laboratory, Los Alamos, NM
G. Kulcinski, University of Wisconsin, Madison, WI
H. Maekawa, Japan Atomic Energy Research Institute, Japan
S. Malang, Forschungszentrum Karlsruhe, Karlsruhe, Germany
D. Markovskij, Kurchatov Institute, Moscow Russia
W. Marton, U.S. Department of Energy, Germantown, MD
Y. Martynenko, Kurchatov Institute, Moscow, Russia
S. Matsuda, Japan Atomic Energy Research Institute, Naka, Japan
K. McCarthy, Idaho National Engineering and Environmental Laboratory, Idaho Falls, ID
R. Miller, University of California, San Diego, CA
R. Moir, Lawrence Livermore National Laboratory, Livermore, CA
F. Najmabadi, University of California, San Diego, CA
A. Opdenaker, U.S. Department of Energy, Germantown, MD
R. Parker, Massachusetts Institute of Technology, Cambridge. MA
K. Pasamehmetoglu, Los Alamos National Laboratory, Los Alamos, NM
J. Perkins, Lawrence Livermore National Laboratory, Livermore, CA
D. Petti, Idaho National Engineering and Environmental Laboratory, Idaho Falls, ID
E.J. Pitcher, Los Alamos National Laboratory, Los Alamos, NM
C. Rodriguez, General Atomics, San Diego, CA
M. Sawan, University of Wisconsin, Madison, WI
K. Schultz, General Atomic, San Diego, CA
G. Shatalov, Kurchatov Institute of Atomic Energy, Moscow, Russia
M. Solonin, Bochvar Research Institute of Inorganic Materials, Moscow, Russia
W.M. Stacey, Georgia Institute of Technology, Atlanta, GA
D. Steiner, Rensselaer Polytechnic Institute, Troy, NY
Y. Strebkov, Research and Development Institute of Power Engineering, Moscow, Russia
I. Sviatoslavsky, University of Wisconsin, Madison, WI
M. Tillack, University of California, San Diego, CA
M. Todosow, Brookhaven National Laboratory, Upton, L.I., NY
H. Trellue, Los Alamos National Laboratory, Los Alamos, NM
G.J. Van Tuyle, Los Alamos National Laboratory, Los Alamos, NM
E.P. Velikov, Kurchatov Institute of Atomic Energy, Moscow, Russia
C. Wong, General Atomics, San Diego, CA
C.E.A. Library, Fontenay-aux-Roses, France
Librarian, Culham Laboratory, England
Thermonuclear Library, Japan Atomic Energy Research Institute, Japan
University of Illinois, Fusion Studies Laboratory
University of Illinois, Grainger Engineering Library Information Center